

Identifying Drift, Diffusion, and Causal Structure from Temporal Snapshots

Vincent Guan¹ Joseph Janssen¹ Hossein Rahmani¹ Andrew Warren¹
 Stephen Zhang² Elina Robeva¹ Geoffrey Schiebinger¹

¹University of British Columbia

²University of Melbourne

October 30, 2024

Abstract

Stochastic differential equations (SDEs) are a fundamental tool for modelling dynamic processes, including gene regulatory networks (GRNs), contaminant transport, financial markets, and image generation. However, learning the underlying SDE from observational data is a challenging task, especially when individual trajectories are not observable. Motivated by burgeoning research in single-cell datasets, we present the first comprehensive approach for jointly estimating the drift and diffusion of an SDE from its temporal marginals. Assuming linear drift and additive diffusion, we prove that these parameters are identifiable from marginals if and only if the initial distribution is not invariant to a class of generalized rotations, a condition that is satisfied by most distributions. We further prove that the causal graph of any SDE with additive diffusion can be recovered from the SDE parameters. To complement this theory, we adapt entropy-regularized optimal transport to handle anisotropic diffusion, and introduce APPEX (Alternating Projection Parameter Estimation from X_0), an iterative algorithm designed to estimate the drift, diffusion, and causal graph of an additive noise SDE, solely from temporal marginals. We show that each of these steps are asymptotically optimal with respect to the Kullback–Leibler divergence, and demonstrate APPEX’s effectiveness on simulated data from linear additive noise SDEs.

1 Introduction

This work presents the first comprehensive approach for jointly estimating the drift and diffusion of a stochastic differential equation (SDE) from observed temporal marginals. While parameter estimation has been studied extensively using trajectory data, either given one long trajectory [BPRF06, NMY00, Bis07, TB13, MMP15, KOLL12, NR20, CHLS23], or multiple short trajectories [MCF⁺24, WGH⁺24, LJP⁺21, PHR19, NM24], it is often impossible to observe individual trajectories when tracking large populations. For example, in single-cell RNA sequencing (scRNA-seq) datasets, the destructive nature of sequencing technologies prevents specific cells from being tracked over time [TCG⁺14, STRZ⁺16, FWR⁺18, SST⁺19, LZKS21]. Similarly, hydrogeochemical sensors cannot track distinct particles when studying contaminant flow, providing only data on plume migration [MT07, HZL⁺23, SFGGH07, Elf06, AG92, BYB⁺92, MFRC86]. Observational data may therefore be limited to samples from temporal marginals of the process at various measurement times. We refer to this observational setting as *marginals-only*.

However, many distinct stochastic processes are known to be indistinguishable under the marginals-only setting [WWT⁺18, CHS22]. Due to these non-identifiability concerns, previous works simplify the problem significantly, such that at least one of diffusion or drift are already known [LZKS21, SBB24b, VTLL21, CZHS22, Zha24, For24]. Moreover, it is common to impose model restrictions, such as irrotational drift and isotropic diffusion [LZKS21, CZHS22, Zha24, SBB24b, VTLL21, WWT⁺18]. In this work, we prove in Theorem 4.3 that non-identifiability under the time-homogeneous linear additive noise SDE model is resolved if the initial distribution X_0 is not auto-rotationally invariant (see Definition 4.2). We further introduce a practical method for estimating the drift and diffusion of a general additive noise process, without prior knowledge or additional assumptions, and extensively demonstrate its effectiveness on simulated data.

1.1 Background and related work

SDEs have long been used to model natural processes [OT10, DAD05, LES03, SST⁺19], where the drift and diffusion have meaningful physical interpretations. In single-cell biology, the drift and diffusion model cell differentiation, where a stem cell changes into another cell type, such as a blood cell or bone cell. This process is often visualized with Waddington’s epigenetic landscape, where cells figuratively traverse a developmental terrain, guided by deterministic forces (drift) and stochastic fluctuations (diffusion) [Wad35, Wad57, SST⁺19]. In particular, the drift can be related to the set of genes that directly regulate the expression of a gene of interest [Zha24, AVI⁺20, ATW⁺24, ZLSS24, TLBB⁺23], and therefore provides insights into genetic diseases and gene therapies. Meanwhile, the diffusion informs the extent to which cell fates are determined by initial conditions [For24]. In hydrological systems, drift is linked to important and unknown properties of the subsurface, such as hydraulic conductivity through average flow velocity [HZL⁺23, BHR93], while the diffusion usually describes material heterogeneity or turbulence [BHR93], and therefore informs the applicability of popular models, such as Darcy’s law [MT07, OT10, LKR02]. Together, these parameters determine pollutant fates in hydrological systems, a key concern in safeguarding drinking water sources [O⁺02, FMR06, LBSV⁺19, CCMV99, Pau97, CBL⁺19]. In some models, drift and diffusion are also directly dependent on one another, as in the chemical Langevin equation [Gil00] and the advection-dispersion equation for solute transport [HZL⁺23, LKR02, BHR93]. We remark that even when the drift and diffusion are independent, these parameters remain inextricably linked, as they jointly explain the dynamics of the underlying process.

Inference from temporal marginals. The marginals-only observational setting dates back to at least Aristotle, who inferred the processes and mediators (e.g., heat) behind embryogenesis by dissecting bird eggs at various stages of development [Wad35, O⁺82, Ari42]. Most contemporary research in this area now focuses on single-cell biology. Many works focus on trajectory inference [SST⁺19, LZKS21, YWI⁺23, CZHS22], while others infer the causal graph, e.g. GRN [AVI⁺20, BLL⁺20, TLBB⁺23, RCM⁺24], or perform parameter estimation [CML09, SBB24a]. Recent research jointly estimates a subset of these quantities by leveraging their intrinsic relationships. For instance, [VTLL21, SBB24b] are primarily interested in trajectory inference, and iteratively estimate drift and trajectories. Meanwhile, [Zha24] iteratively estimates drift and trajectories, while additionally applying permanent interventions on the drift dynamics for network inference.

Due to the difficulty of the problem, most approaches assume that the underlying diffusion is known [LZKS21, SBB24b, VTLL21, CZHS22, Zha24]. Alternatively, [For24] estimates diffusion, but assumes that an accurate estimate of drift is known. However, knowing drift or diffusion *a priori* is unrealistic in practice. In these settings, an accurate guess of one or the other parameter set is crucial because misspecified diffusion typically leads to poor drift estimation and vice-versa [BHR93]. It is also standard to assume that the drift is a conservative field $\nabla\psi$ [WWT⁺18, LZKS21, VTLL21, CZHS22, SBB24b], and that the diffusion is given by isotropic Brownian motion σdW_t [WWT⁺18, LZKS21, VTLL21, CZHS22, Zha24, SBB24b]. However, these constraints impose unrealistic conditions on the data. A conservative drift field cannot model negative feedback loops or repressilator dynamics [WWT⁺18], and isotropic diffusion cannot model different noise scales across variables or latent confounders [RCM⁺24, MH22]. Finally, it is common to leverage additional perturbational data from interventions [RCM⁺24, Zha24], or impose regularization [Zha24] to learn the system more completely. In contrast, given an initial distribution, which is not auto-rotationally invariant, we show that we can jointly estimate the drift, diffusion, and causal graph of any linear additive noise SDE, solely from observational temporal marginals.

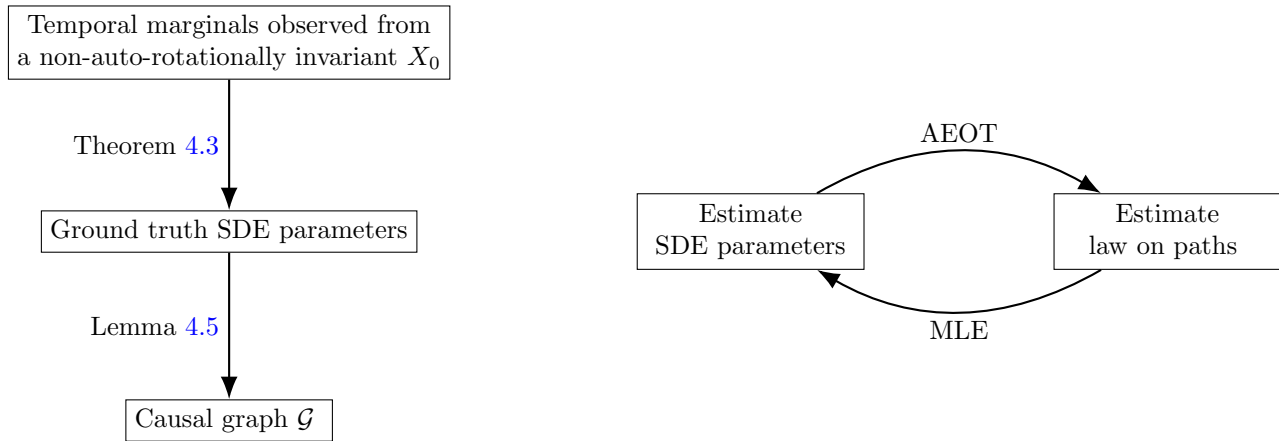
Identifiability. Previous assumptions on prior knowledge and the underlying model are largely attributed to sources of non-identifiability introduced by the marginals-only observational setting [WWT⁺18, CHS22, LZKS21, For24]. Establishing sufficient conditions for identifiability are therefore required to ensure that inference is feasible. [WGH⁺24] showed that identifiability of a time-homogeneous linear additive noise SDE from ground truth trajectories with fixed $X_0 \in \mathbb{R}^d$ is equivalent to a non-degenerate rank condition based jointly on X_0 , and the SDE parameters, given by the linear drift matrix A and the observational diffusion GG^T . In contrast, our work studies identifiability of linear additive noise SDEs in the more general setting of observing temporal marginals. As detailed in Section 3, the set of non-identifiable systems within our observational setting is strictly larger. Furthermore, we demonstrate that identifiability for linear additive noise SDEs can be guaranteed with a wide class of initial distributions. To the best of our knowledge, this has not been shown even in the case of trajectory-based observations.

By connecting SDE parameter identification to recent work on dynamic structural causal models [BM24],

we show that full causal identification is possible from the linear additive noise SDE model, if the initial distribution X_0 is not auto-rotationally invariant. This implies non-Gaussianity of the initial marginal, which is reminiscent of linear non-Gaussian acyclic models, where the full causal graph is identifiable [SHH⁺06].

1.2 Our contributions

In this work, we show that it is possible to infer the drift, diffusion, and underlying causal graph, solely from appropriately initialized temporal marginals. We illustrate our theoretical contributions in Figure 1a and our algorithmic contributions in Figure 1b. We further outline our contributions below said figures.



(a) Theoretical contributions: identifying drift, diffusion, and causal structure from temporal marginals

(b) Algorithmic contributions: APPEX algorithm

Figure 1: Outline of our theoretical (a) and algorithmic (b) contributions. In (b), our algorithm Alternating Projection Parameter Estimation from X_0 alternates between Anisotropic Entropy-regularized Optimal Transport (AEOT) and Maximum Likelihood Estimation (MLE).

1. We provide a theoretical foundation for system identification from temporal marginals in Section 4.
 - (a) In Theorem 4.3, we provide a full characterization of the identifiability conditions for the drift and diffusion parameters from temporal marginals, under the time-homogeneous linear additive noise model. Identifiability is guaranteed if and only if the initial distribution X_0 is not auto-rotationally invariant (see Definition 4.2).
 - (b) In Lemma 4.5, we connect parameter estimation to causal structure learning via dynamic structural causal models [BM24]. We show that the causal graph of any additive noise model can be recovered from the SDE parameters.
2. In Section 5, we introduce our algorithm: Alternating Projection Parameter Estimation from X_0 (APPEX). It is the first method designed to estimate drift and diffusion from temporal marginals of additive noise SDEs, without prior knowledge.
 - (a) We show that with each iteration, APPEX’s estimates approach the true solution. APPEX alternates between a trajectory inference step, which is a Schrödinger bridge problem, and a parameter estimation step, which is solved via maximum likelihood estimation. We show that both sub-procedures are optimal with respect to the Kullback-Leibler (KL) divergence.
 - (b) To solve the associated Schrödinger bridge problem for trajectory inference, given arbitrary additive noise, we adapt entropic optimal transport for parameter dependent transport costs, including anisotropic diffusion.
 - (c) We test APPEX’s efficacy across a wide range of experiments in Section 6. APPEX can identify the drift and diffusion parameters from the previously non-identifiable examples introduced in Section 3, if given appropriate non-auto-rotationally invariant initial distributions. We also demonstrate APPEX’s effectiveness over a large-scale experiment on higher dimensional SDEs with randomly

generated parameter sets. Our results demonstrate that APPEX identifies arbitrary linear additive noise SDEs with significantly higher accuracy than the widely-used Waddington-OT (WOT) method [SST⁺19]. Our final experiments demonstrate that APPEX can be used to identify the system’s causal graph, even in the presence of latent confounders.

2 Mathematical setup

Let $b(X_t)$ be a Lipschitz function $b : \mathbb{R}^d \rightarrow \mathbb{R}^d$, $G \in \mathbb{R}^{d \times m}$, and denote the standard m -dimensional Brownian motion as $W_t \in \mathbb{R}^m$. $X_t \in \mathbb{R}^d$ is the solution to the corresponding time-homogeneous additive noise SDE if

$$dX_t = b(X_t) dt + G dW_t, \quad X_0 \sim p_0. \quad (1)$$

The condition that $b(X_t)$ is a Lipschitz drift function ensures existence and uniqueness of the SDE solution [FG20]. The additive noise is modeled by the diffusion matrix $G \in \mathbb{R}^{d \times m}$. In this paper, we also refer to $H = GG^\top \in \mathbb{R}^{d \times d}$ as the (observational) diffusion, since it is only possible to observe H [WGH⁺24, Pav14].

Time-homogeneous linear additive noise SDEs are among the most studied SDEs, and have been applied to numerous fields of interest [WGH⁺24]. These SDEs generalize the popular Ornstein-Uhlenbeck process, such that stationarity is not assumed. A time-homogeneous linear additive noise SDE obeys the form

$$dX_t = AX_t dt + G dW_t, \quad X_0 \sim p_0, \quad A \in \mathbb{R}^{d \times d} \quad (2)$$

The primary objective of this paper is to estimate the drift and diffusion parameters of the SDE from temporal marginals. Given an SDE, a temporal marginal is the distribution of the process at time t , which we denote by $p_t \sim X_t$. In particular, given N observed measurement times $t_0 = 0, \dots, t_{N-1}$, we would like to estimate the drift and diffusion of the SDE given the set of measured marginals $\{p_i\}_{i=0}^{N-1}$. For a linear additive noise SDE, this corresponds to identifying A and $H = GG^\top$ from $\{p_i\}_{i=0}^{N-1}$.

The Fokker-Planck equation (3) describes the continuous evolution of the process’ temporal marginals p_t from the initial distribution p_0 . A straightforward computation shows that the marginals of a linear additive noise SDE evolve according to the following Fokker-Planck equation:

$$\frac{\partial}{\partial t} p(x, t) = -\nabla \cdot (Ax)p(x, t) + \frac{1}{2} \nabla \cdot (H \nabla p(x, t)), \quad p(x, 0) = p_0(x). \quad (3)$$

Although (3) assumes differentiability, we note that it can also be defined in the weak distributional sense for general probability measures p_t (see Appendix Section 8.2).

In the finite sample setting, we observe M_i samples for the i th marginal. The empirical marginal distribution is given by $\hat{p}_i \sim \text{Unif}\{x_{t_i}^{(j)} : j \in 1, \dots, M_i\}$, where $x_{t_i}^{(j)}$ is the j th observation of the process at time t_i . If we take the number of observations M_i per time to be infinite, then our observed marginals \hat{p}_i would equal the true marginal distributions p_i of the SDE.

Notation	Meaning
$b(X_t)$	Drift function of a general SDE
A	Drift matrix of a linear SDE
G	Diffusion matrix of an additive noise SDE
$H = GG^\top$	Observational diffusion matrix
$p_t \sim X_t$	Temporal marginal distribution of the SDE at time t
$p(x, t)$	Probability density of the process at time t , assuming existence
$X_i = X_{t_i}$	Distribution of SDE at i th observation time
ΔX_i	$X_{i+1} - X_i$
$p_i \sim X_{t_i}$	Temporal marginal distribution of the SDE at measured time t_i
N	Number of observed temporal marginals
\hat{p}_i	Empirical temporal marginal of the SDE at measured time t_i
$x_{t_i}^{(j)}$	j th sample from i th empirical marginal
M_i	Number of samples for the i th empirical temporal marginal \hat{p}_i
Σ	Covariance of an initial distribution X_0
ϵ	Scalar parameter for regularizing entropy-regularized optimal transport (EOT)
$\Sigma(\theta)$	(Possibly) anisotropic matrix parameter for regularizing anisotropic entropy regularized optimal transport (AEOT)

We note that estimating the drift and diffusion amounts to determining the law on paths of the process' trajectories. Indeed, if the process has bounded second moments, and is defined by a Lipschitz drift function and nondegenerate diffusion, then the process admits a density with respect to the Wiener measure over the path space $\Omega = C([0, T], \mathbb{R}^d)$ [Oks13, SBB24b]. Moreover, trajectories evolve according to the transition kernel, which can be approximated for additive noise SDEs with $X_{t+\Delta t}|X_t \sim \mathcal{N}(X_t + b(X_t)\Delta t, H\Delta t)$ [SBB24b, Pav14]. The exact transition kernel of a linear additive noise SDE is given by $X_{t+\Delta t}|X_t \sim \mathcal{N}(\mu_t, \Sigma_t)$, where $\mu_t = e^{A\Delta t}X_t$ and $\Sigma_t = \int_t^{t+\Delta t} e^{A(t-s+\Delta t)}He^{A^\top(t-s+\Delta t)}ds$ [Zha24], and can practically be estimated via $\mathcal{N}(X_t + AX_t\Delta t, H\Delta t)$.

3 Examples of non-identifiability

The problem of non-identifiability given p_0 appears if there exists an alternative drift-diffusion pair, $(\tilde{A}, \tilde{H}) \neq (A, H)$, which shares the same time marginals, following initial distribution $X_0 \sim p_0$. Equivalently, the processes share the same Fokker-Planck equation (3) across all observed times. We first summarize a few classical examples of non-identifiability from the literature [LZKS21, SBB24b, WGH+24, HGJ16, WWT+18]. In all examples, the processes X_t and Y_t share the same time marginals.

Example 3.1 (Starting at stationary distribution [LZKS21, SBB24b]). *This example is motivated by the fact that multiple SDEs may share the same stationary distribution. Hence, if p_0 is initialized at the stationary distribution, then each of these SDEs will be non-identifiable from their marginals. We provide a simple example.*

$$dX_t = -X_t dt + dW_t, \quad X_0 \sim \mathcal{N}(0, \frac{1}{2}) \quad (4)$$

$$dY_t = -10Y_t dt + \sqrt{10}dW_t, \quad Y_0 \sim \mathcal{N}(0, \frac{1}{2}) \quad (5)$$

Here, both SDEs have the same stationary distribution $\mathcal{N}(0, \frac{1}{2})$ despite having significantly different individual trajectories. Indeed, the stationary distribution of a 1-dimensional 0-mean Ornstein-Uhlenbeck (OU) process with drift $-\lambda X_t$ and diffusion σ is $\mathcal{N}(0, \frac{\sigma^2}{2\lambda})$, which depends only on the drift:diffusivity ratio λ/σ^2 [LZKS21]. For multivariate OU processes with drift A and observational diffusion H , the stationary distribution $\mathcal{N}(0, \Sigma)$ depends only on the relationship $\Sigma A + A\Sigma = -H$ [MHB16]. Intuitively, the set of OU processes, which share the same stationary distribution $\mathcal{N}(0, \Sigma)$ are equivalent up to rescaling time.

Example 3.2 (Rotation around process mean [SBB24b, HGJ16, WWT+18]). *In this example, the first SDE governing X_t is 2-dimensional Brownian motion and the second SDE governing Y_t adds a divergence-free rotational vector field $(x, y) \rightarrow (y, -x)$ about $(0, 0)$, which is undetectable if the initial distribution p_0 is rotationally invariant.*

$$dX_t = dW_t, \quad X_0 \sim \mathcal{N}(0, Id) \quad (6)$$

$$dY_t = \begin{bmatrix} 0 & 1 \\ -1 & 0 \end{bmatrix} Y_t dt + dW_t, \quad Y_0 \sim \mathcal{N}(0, Id) \quad (7)$$

Hence, if p_0 is an isotropic distribution with mean $(0, 0)$, then X_t and Y_t are non-identifiable from one another [SBB24b]. This can also be shown directly with the Fokker-Planck equation (3), since $\nabla \cdot (Ax)p(x, t) = \nabla p(x, t) \cdot Ax + p(x, t)\nabla \cdot A(x) = \nabla p(x, t) \cdot Ax = 0$, if p is parallel to the rotational vector field $Ax = \begin{bmatrix} 0 & 1 \\ -1 & 0 \end{bmatrix} x$.

Example 3.3 (Degenerate rank [WGH+24]). *In this example motivated by [WGH+24], trajectories (and therefore temporal marginals) of distinct SDEs are non-identifiable if the process is degenerate, limiting observations to a strict subspace of \mathbb{R}^d .*

$$dX_t = \begin{bmatrix} 1 & 2 \\ 1 & 0 \end{bmatrix} X_t dt + \begin{bmatrix} 1 & 2 \\ -1 & -2 \end{bmatrix} dW_t, \quad X_0 = \begin{bmatrix} 1 \\ -1 \end{bmatrix} \quad (8)$$

$$dY_t = \begin{bmatrix} 1/3 & 4/3 \\ 2/3 & -1/3 \end{bmatrix} Y_t dt + \begin{bmatrix} 1 & 2 \\ -1 & -2 \end{bmatrix} dW_t, \quad Y_0 = \begin{bmatrix} 1 \\ -1 \end{bmatrix} \quad (9)$$

The drift matrices $\begin{bmatrix} 1 & 2 \\ 1 & 0 \end{bmatrix}, \begin{bmatrix} 1/3 & 4/3 \\ 2/3 & -1/3 \end{bmatrix}$ each have eigenvector $X_0 = \begin{bmatrix} 1 \\ -1 \end{bmatrix}$ with eigenvalue -1 . Moreover, the diffusion is rank-degenerate with column space $\text{span}\left(\begin{bmatrix} 1 \\ -1 \end{bmatrix}\right)$. Thus, both SDEs will have identical behaviour along $\text{span}\left(\begin{bmatrix} 1 \\ -1 \end{bmatrix}\right)$ and are only differentiated by their behaviour elsewhere. Given $X_0 = \begin{bmatrix} 1 \\ -1 \end{bmatrix}$, the processes will stay within $\text{span}\left(\begin{bmatrix} 1 \\ -1 \end{bmatrix}\right)$ and are non-identifiable from one another. We note that this non-identifiability holds even when we observe trajectories [WGH⁺24], whereas the first two examples are identifiable from trajectories but not identifiable from marginals.

In order to contend with these sources of non-identifiability, the standard assumptions are that the drift is an irrotational vector field and that the diffusion is both known and isotropic [WWT⁺18, LZKS21, CZHS22, SBB24b]. The primary goal of Section 4.1 is to show when the SDE parameters are identifiable without such assumptions. We discuss the restrictive implications of previous assumptions in Section 4.2.

4 System identification from temporal marginals

We provide a full characterization of the conditions for identifiability of linear additive noise SDEs from observed time marginals in Section 4.1. In particular, identifiability is determined by generalized rotational properties of the initial distribution X_0 , for which we provide preliminary definitions below. We then show in Section 4.2 that one can recover the underlying causal graph from the identified parameters of a general additive noise SDE.

Definition 4.1. We define a Σ -generalized rotation in \mathbb{R}^d as the matrix exponential e^{At} , such that $A \in \mathbb{R}^{d \times d}$ is skew-symmetric with respect to $\Sigma \succeq 0$, i.e. $A\Sigma + \Sigma A^\top = 0$. In particular, if the rotation is applied to a r.v. X with covariance Σ , then the covariance will be preserved, i.e. $\Sigma = \text{Cov}(X) = \text{Cov}(e^{At}X)$ (Lemma 8.5 in Appendix).

$\Sigma = \gamma I_d$ defines classical rotations, such that spheres, e.g. $S^{d-1} = \{x \in \mathbb{R}^d : \gamma x^\top x = 1\}$, are rotationally invariant. For anisotropic choices of Σ , ellipsoids, e.g. $E_\Sigma = \{x \in \mathbb{R}^d : x^\top \Sigma^{-1} x = 1\}$, are rotationally invariant. If $\Sigma \succ 0$, then Σ -generalized rotations can be interpreted as classical rotations within the Σ -weighted inner product space \mathbb{R}_Σ^d , since they preserve the norm $\|x\|_\Sigma^2 = x^\top \Sigma^{-1} x$.

Definition 4.2. Let X be a d -dimensional r.v. with covariance Σ . We say that X is auto-rotationally invariant, if there exists a nontrivial Σ -generalized rotation e^{At} with $A \neq 0$ such $e^{At}X \sim X \forall t \geq 0$. Conversely, X is not auto-rotationally invariant, if $e^{At}X \sim X \forall t \geq 0$ admits only the solution $A = 0$.

Auto-rotational invariance can be interpreted as a random variable being rotationally invariant under the geometry induced by its own covariance Σ . For example, Gaussians $\mathcal{N}(0, \Sigma)$ and uniform distributions over ellipsoids are auto-rotationally invariant random variables. Additionally, all rank degenerate r.v.'s are auto-rotationally invariant, since $e^{At}X \sim X$ would be satisfied by any matrix A , such that X is in its nullspace with probability 1. However, given full-dimensional support, auto-rotational invariance requires strict ellipsoidal symmetry on the r.v.'s density (Lemma 8.6 in Appendix), which means that almost all non-degenerate r.v.'s are not auto-rotationally invariant. We provide more examples and theory about rotations in Appendix 8.3, and also refer the reader to [Özd16] for additional theory about elliptical rotations.

4.1 SDE parameter identifiability

We are now ready for our main identifiability theorem, which characterizes identifiability of linear additive noise SDEs.

Theorem 4.3. Let X_t evolve according to a d -dimensional time-homogeneous linear additive noise SDE (2), with initial condition $X_0 \sim p_0$, such that all the moments of p_0 are finite. Then, the drift A and the diffusion GG^\top of the SDE can be uniquely identified from the time marginals p_t if and only if $X_0 \sim p_0$ is not auto-rotationally invariant.

Proof. We present the proof in the case where p_t has smooth density $p(x, t)$. The analogous argument for the case where p_t is any probability measure is included in Appendix 8.3.

We first show that if X_0 is auto-rotationally invariant, then there exist multiple processes with distinct drift-diffusion parameters $(A, H = GG^\top)$, which would share the same time marginals p_t , when initialized at $X_0 \sim p_0$. Let X_0 be an auto-rotationally invariant r.v. with $\text{cov}(X_0) = \Sigma$. Then, there exists a matrix $A \neq 0$ such that $e^{As}X_0 \sim X_0 \forall s \geq 0$. To define the non-identifiable SDEs, the idea is to generalize the non-identifiable isotropic rotation example (3.2). In particular, we will define the non-identifiable SDEs such that only one of the SDEs has nonzero drift A , and both SDEs have diffusion proportional to $GG^\top = \Sigma$. We will prove that for all $\gamma \in \mathbb{R}$, the SDEs

$$dX_t = \gamma G dW_t \quad (10)$$

$$dX_t = AX_t dt + \gamma G dW_t \quad (11)$$

will have the same time marginals $p(x, t)$. The Fokker-Planck equations for the two SDEs are given by

$$\frac{\partial}{\partial t} p(x, t) = \frac{\gamma^2}{2} \nabla \cdot (\Sigma \nabla p(x, t)) \quad p(x, 0) = p_0(x), \quad (12)$$

$$\frac{\partial}{\partial t} p(x, t) = -\nabla \cdot (Ax)p(x, t) + \frac{\gamma^2}{2} \nabla \cdot (\Sigma \nabla p(x, t)) \quad p(x, 0) = p_0(x). \quad (13)$$

To show that the processes exhibit the same time marginals, we show that (12) and (13) are equivalent by showing that the first divergence term in (13) is identically zero. We begin by showing equivalence at $t = 0$. We need to show that for all $x \in \mathbb{R}^d$,

$$\nabla \cdot (Ax)p(x, 0) = \nabla p(x, 0) \cdot Ax + p(x, 0) \nabla \cdot (Ax) = 0. \quad (14)$$

By the auto-rotational invariance of X_0 , $p(x, 0)$ satisfies: $p(e^{As}x, 0) = p(x, 0) \forall s$. Taking the derivative with respect to s at $s = 0$ and using chain rule, we have:

$$0 = \left. \frac{d}{ds} p(x, 0) \right|_{s=0} = \left. \frac{d}{ds} p(e^{As}x, 0) \right|_{s=0} = \nabla p(x, 0) \cdot \left. \frac{d}{ds} e^{As}x \right|_{s=0} = \nabla p(x, 0) \cdot Ax,$$

so the first term on the right side of (14) vanishes. We now show $\nabla \cdot (Ax) = \text{tr}(A) = 0$ to prove (14). Lemma 8.5 implies that $A\Sigma + \Sigma A^\top = 0$ and Lemma 8.9 shows that without loss of generality, we may pick A so that $\text{Tr}(A) = 0$. This proves (14) for $t = 0$. The same argument applies for $t > 0$ upon noticing that for both systems, X_t is also auto-rotationally invariant with respect to the same map $e^{As}X_t \sim X_t$. This is shown in the Appendix under Lemma 8.12. This demonstrates that if X_0 is auto-rotationally invariant, then we do not have identifiability from marginals over the class of linear additive noise SDEs.

We now prove that identifiability is guaranteed if X_0 is not auto-rotationally invariant. Suppose that two linear additive noise SDEs with parameters $(A, H = GG^\top)$ and $(\tilde{A}, \tilde{H} = \tilde{G}\tilde{G}^\top)$ have the same time marginals $p(x, t)$ given the same initial distribution $X_0 \sim p_0$, which is not auto-rotationally invariant. We will prove that $(A, H) = (\tilde{A}, \tilde{H})$ must hold. Since both SDEs share the same marginals, their Fokker-Planck equations are equivalent:

$$\frac{\partial}{\partial t} p(x, t) = L(p(x, t)) := -\nabla \cdot (Ax)p(x, t) + \frac{1}{2} \nabla \cdot (H \nabla p(x, t)) \quad p(x, 0) = p_0(x) \quad (15)$$

$$= L_1(p(x, t)) := -\nabla \cdot (\tilde{A}x)p(x, t) + \frac{1}{2} \nabla \cdot (\tilde{H} \nabla p(x, t)) \quad p(x, 0) = p_0(x) \quad (16)$$

By linearity, we may subtract both equations and obtain

$$0 = (L - L_1)(p(x, t)) = -\nabla \cdot (\tilde{A}x)p(x, t) + \frac{1}{2} \nabla \cdot (\tilde{H} \nabla p(x, t)) \quad p(x, 0) = p_0(x), \quad (17)$$

where $\tilde{A} = A - \tilde{A}$ and $\tilde{H} = H - \tilde{H}$. Hence, p_0 is a stationary solution to (17), such that $p_t = p_0$ for all $t \geq 0$. Now, (17) is precisely the Fokker-Planck equation for the *residual* SDE, which is the linear additive noise SDE given by

$$dX_t = \tilde{A}X_t dt + \tilde{G}dW_t, \quad (18)$$

such that $\bar{G}\bar{G}^\top = \bar{H}$. $X_t \sim X_0 \forall t \geq 0$. Then, we note that if $\bar{H} \neq 0$, (18) can only admit a Gaussian stationary distribution. In particular, stationarity would require that (18) is an Ornstein-Uhlenbeck process [Doo42], whose stationary distribution is $\mathcal{N}(0, \Sigma)$, where $\Sigma\bar{A} + \bar{A}\Sigma = -\bar{H}$ [MHB16]. Thus, if X_0 is not auto-rotationally invariant, then X_0 is non-Gaussian, and we must conclude that $\bar{H} = H - \tilde{H} = 0$. Furthermore, this implies that the residual SDE is deterministic, such that

$$\frac{dX_t}{dt} = \bar{A}X_t \implies X_t = e^{\bar{A}t}X_0 \quad (19)$$

$$X_t = e^{\bar{A}t}X_0 \sim X_0 \quad \forall t \geq 0. \quad (20)$$

However, note that $e^{\bar{A}t}X_0 \sim X_0$ admits only the trivial solution $\bar{A} = 0$ since X_0 is not auto-rotationally invariant. This proves that $A = \bar{A}$ and $H = \bar{H}$ as desired. \square

Theorem 4.3 tells us that identifiability from marginals is guaranteed if the initial distribution X_0 is not auto-rotationally invariant. Conversely, if X_0 is auto-rotationally invariant, then it is possible to construct multiple SDEs with the same ensuing marginals. However, we note that in practice, observed marginals may not be compatible with our constructed example (11). An open question is if non-identifiability persists given any set of observed marginals, which start from an auto-rotationally invariant distribution X_0 . As discussed previously, most distributions are not auto-rotationally invariant, and are hence conducive to identifiability. Figure 2 demonstrates how non-auto-rotationally invariant initial distributions X_0 resolve the non-identifiability of temporal marginals from the examples in Section 4. We discuss this in Appendix 8.4.

4.2 Causal graph identification

Given that the drift and diffusion are identified, we can gain important insights into the system's causal structure. It has already been shown that knowing drift and diffusion provides the system's post-intervention distributions [HS14, WGH+24]. We will prove that under basic conditions, we can recover the causal graph \mathcal{G} of an additive noise SDE from the drift $b(X_t)$ and observational diffusion $H = GG^\top$.

We first review how a causal graph can be defined from an SDE. Consider a d -dimensional additive noise SDE (1). By isolating the j th variable and integrating, we obtain:

$$X_t^{(j)} = X_0^{(j)} + \int_0^t b_j(X_s^{\alpha(j)}) ds + \sum_{k=1}^m G_{j,k} W_t^{(k)}, \quad (21)$$

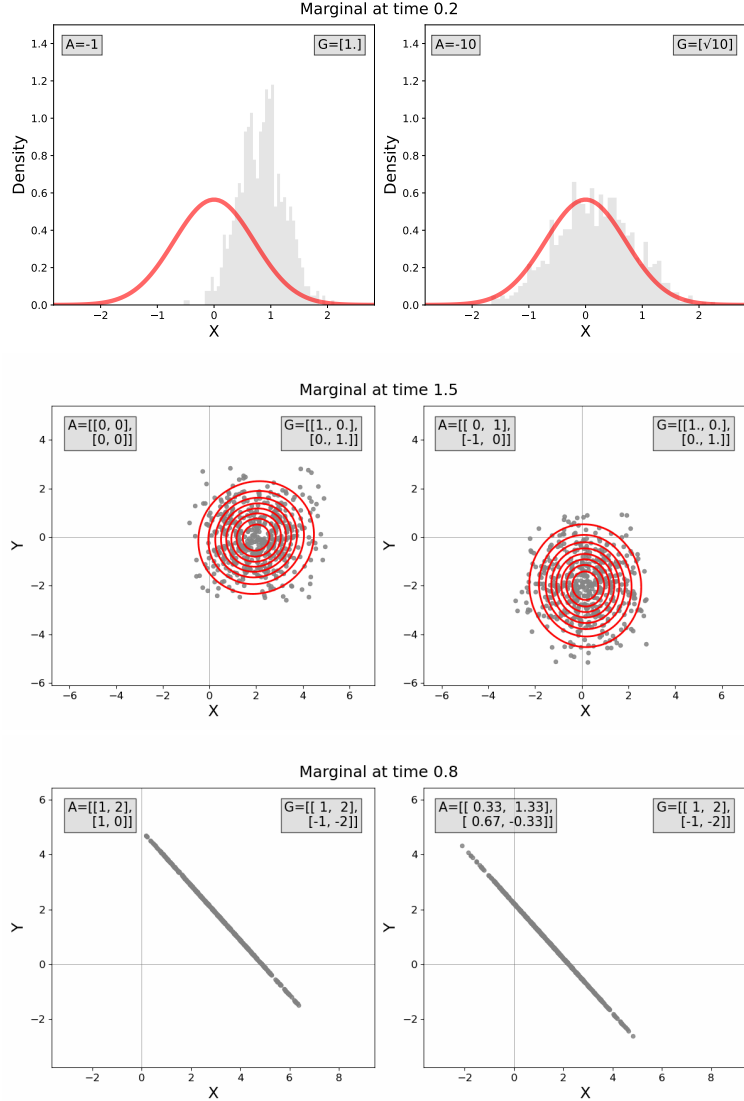
where W_t is an m -dimensional Brownian motion, $\alpha(j) \subset [d]$ is the set of variables that are used as input in $b_j(X_t)$. Then, (21) is an example of a dynamic structural causal model [BM24]. In particular, we can define a causal graph \mathcal{G} over vertices $V = [d]$ and edges $E = \{i \rightarrow j : j \in [d], i \in \alpha(j)\}$ [BM24][Definition 2]. Intuitively, given $j \in V$, we include the edge $i \rightarrow j$ if $X^{(i)}$ influences the evolution of variable $X^{(j)}$ through the drift. We note that in non-additive noise models, edges $i \rightarrow j$ can also be formed due to the diffusion. In this paper, we assume that latent confounders are modeled with shared driving noise.

Definition 4.4. *Let X evolve according to a d -dimensional additive noise SDE: $dX_t = b(X_t)dt + GdW_t$. We define a multi-directed edge $\tilde{e} = (i_1, \dots, i_p) \in \mathcal{G}$ if variables $X^{(i_1)}, \dots, X^{(i_p)}$ depend on a common noise source $W_t^{(k)}$, $k \in [m]$. To explicitly represent the latent confounder, one may also use the alternative graphical representation of adding the vertex U_{i_1, \dots, i_p} , with directed edges pointing to each of i_1, \dots, i_p (as done in [HSKP08]).*

This definition is motivated by [LRW21], where multidirected edges represent sets of variables, which share a hidden latent confounder. We also note that it is common to model latent confounders with correlated diffusion in the dynamic setting (see [LKS24, MH22], and [BM24][Example 4]).

Lemma 4.5. *Let X_t evolve according to a d -dimensional additive noise SDE: $dX_t = b(X_t) dt + GdW_t$, and let $\mathcal{G} = (V = [d], E, \tilde{E})$ be its causal graph, over the variables $X^{(1)}, \dots, X^{(d)}$, with directed edge set E and multidirected edge set \tilde{E} .*

- a. *There exists a directed edge $e = i \rightarrow j$ in \mathcal{G} if and only if $b_j(X_t)$ depends on $X_t^{(i)}$.*
- b. *There exists a multidirected edge \tilde{e} containing (i, j) in \mathcal{G} , if and only if $H_{i,j} = (GG^\top)_{i,j} \neq 0$.*



(a) This corresponds to Example 3.1 with $X_0 \sim \delta_1$. The SDE with drift $A = H = 10$ (right) has converged to the stationary distribution (red) at time $t = 0.2$, while the SDE with $A = H = 1$ (left) has not yet sufficiently drifted or diffused.

(b) This corresponds to Example 3.2, with $X_0 \sim \text{Unif}\{(2, 0), (2, 0.1)\}$. The first SDE is irrotational and maintains mean $(2, 0.05)$. The second SDE (right) rotates about the origin. At time $t = 1.5$, the mean has shifted to approximately $(0, -2)$.

(c) This corresponds to Example 3.3, with $X_0 \sim \text{Unif}\{(1, 0)^\top, (0, 1)^\top\}$. The first SDE (left) has eigenvalue 2 for $(2, 1)$, while the second (right) has eigenvalue 1, leading to more extreme intercepts in the left plot at $t = 0.8$.

Figure 2: Marginals are plotted at various times for the SDE pairs from Section 4 following various non-rotationally invariant initial distributions.

Thus, \mathcal{G} is fully identified by $b(X_t)$ and $H = GG^\top$ if no more than two observed variables share a common noise source.

Proof. The first claim follows immediately from the definition of the dynamic structural causal model (21).

To prove the second claim, it is easy to see from (21) that $X^{(i_1)}, \dots, X^{(i_p)}$ depends on a common noise source if and only if $G_{i_1, k}, \dots, G_{i_p, k} \neq 0$ for some column $k \in [m]$ in the diffusion G . Indeed, the existence of such a column implies that $X^{(i_1)}, \dots, X^{(i_p)}$ each depend on $W_t^{(k)}$, and the other direction is given by the fact that W_t is a multivariate Gaussian process, with independent components. If two variables share a noise source, this condition is equivalent to $H_{i, j} = G_i \cdot G_j \neq 0$. We therefore conclude that there is a multidirected edge containing (i, j) in \mathcal{G} iff $H_{i, j} \neq 0$. \square

Although the observational diffusion $H = GG^\top$ informs the presence of latent confounders between pairs of variables, we note that it is impossible for H alone to determine general multidirected edges (i_1, \dots, i_p) over $p > 2$ components, which indicate an unobserved confounder of $X_t^{(i_1)}, \dots, X_t^{(i_p)}$. Indeed, given only $H = GG^\top$, multiple causal interpretations may be possible, because structurally different matrices G, \tilde{G} can obey $H = GG^\top = \tilde{G}\tilde{G}^\top$. We provide an example in Example 8.1 of the Appendix, where we cannot

distinguish between a single multidirected edge $(1, 2, 3)$, and three pairs of bidirected edges $(1, 2)$, $(1, 3)$, $(2, 3)$. Furthermore, we note that shared driving noise is not a comprehensive characterization of latent confounders in the dynamic setting, since confounding effects cannot always be absorbed into the diffusion. For an in depth overview of general dynamic structural causal models and their relation to defining causal graphs, we refer the reader to Appendix 8.1 and references [HS14, MH22, BM24].

Despite these limitations, Lemma 4.5 highlights the power of drift-diffusion identification towards recovering the causal graph. Indeed, the proposition accommodates any stochastic process with additive noise, and is thus equipped to handle complex deterministic relationships between variables, including feedback loops. This setting is particularly well suited for inferring GRNs, which are commonly modeled via additive noise SDEs [WWT⁺18, WTW⁺23, RCM⁺24, Zha24, LZKS21, CZHS22].

The causal framework also highlights the impracticality of common model assumptions within the scRNA-seq literature, namely isotropic diffusion $H = GG^T = \sigma^2 I_d$ and irrotational drift $b(X_t) = \nabla\psi$. We have seen in Lemma 4.5 that latent confounders from shared noise can only be modeled with anisotropic diffusion. Moreover, while we expect GRNs to contain feedback loops, i.e. cycles in \mathcal{G} , imposing irrotational drift prevents most cycles from being considered. We show this for the linear additive noise case below.

Lemma 4.6. *Let X_t evolve according to a linear additive noise SDE (2). Then, the drift AX_t is irrotational if and only if A is symmetric, i.e. $A = A^T$.*

Proof. First, we note that for any symmetric matrix A , the vector field Ax can be expressed as the gradient of the scalar potential given by the quadratic form $\phi(x) = x^T Ax/2$ [PP⁺08] [(96)-(97)]. Hence, Ax is irrotational if $A = A^T$.

For the opposite direction, we recall the fact that any gradient field from $\mathbb{R}^n \rightarrow \mathbb{R}^n$ has a symmetric Jacobian [WT74, Cam14]. Since the Jacobian of a linear vector field $Ax : \mathbb{R}^n \rightarrow \mathbb{R}^n$ is A , we conclude that all irrotational linear vector fields from $\mathbb{R}^n \rightarrow \mathbb{R}^n$ are given by symmetric matrices. \square

Lemma 4.6 shows that imposing irrotationality on a linear model is equivalent to imposing a symmetric drift, which determines a symmetric causal graph. However, as illustrated in [WWT⁺18][Fig. 6], symmetric GRNs cannot capture important relationships, such as negative feedback loops or repressilator dynamics. Indeed, consider the 2-cycle $i \leftrightarrow j$. By Lemma 4.5, $i \rightarrow j$ if $A_{j,i} \neq 0$ and $j \rightarrow i$ if $A_{i,j} \neq 0$. However, if the model is irrotational, then by Proposition 4.6, $A_{i,j} = A_{j,i}$, which can only model a positive feedback loop.

To conclude this section, it is important to note that combining Theorem 4.3 and Lemma 4.5 shows that we can identify the full causal structure (e.g., GRN) if and only if X_0 is non-auto-rotationally invariant.

5 Our parameter estimation method

In this section, we introduce our method, Alternating Projection Parameter Estimation from X_0 (APPEX), which estimates a process’ drift, diffusion, and causal graph from observed temporal marginals. Figure 3 illustrates the general strategy of the APPEX algorithm. We focus on the case where the noise GdW_t is additive and the drift $b(X_t) = AX_t : A \in \mathbb{R}^{d \times d}$, is linear (2), since, under these conditions, Theorem 4.3 guarantees identifiability given that X_0 is not auto-rotationally invariant. However, our algorithm is applicable to any parametric drift family. In this section, we give an intuitive explanation at the population level, using the process’ true temporal marginals $p_i \sim X_{t_i}$. In Section 6, we perform experiments using empirical marginals \hat{p}_i , with finite samples per marginal.

Given observed temporal marginals p_0, \dots, p_{N-1} and an initial guess for drift and diffusion $(A^{(0)}, H^{(0)})$, the idea is to use an alternating optimization algorithm to obtain increasingly better estimates for the drift and diffusion matrices. Formally, we consider the spaces

$$\mathcal{D} = \{q : q_0 = p_0, \dots, q_{N-1} = p_{N-1}\} \text{ and} \tag{22}$$

$$\mathcal{A} = \{p : \exists(A, H) \in \mathbb{R}^{d \times d} \times S_{\geq 0}^d \text{ s.t. } p(x, t|y, s) \sim \mathcal{N}(e^{A(t-s)}y, H(t-s))\}, \tag{23}$$

where \mathcal{D} is the set of laws on paths, which coincide with the N temporal marginals at their respective times, and \mathcal{A} is the set of laws given by linear additive noise SDEs. To find the underlying linear additive noise SDE in the intersection $\mathcal{A} \cap \mathcal{D}$, our method will alternate between information projections, $\arg \min_{q \in \mathcal{D}} D_{KL}(q||p)$ and moment projections, $\arg \min_{p \in \mathcal{A}} D_{KL}(q||p)$. Intuitively, the information projection step corresponds to trajectory inference, whose goal is to find the law on paths $q \in \mathcal{D}$, which best aligns with the reference measure p . The moment projection then corresponds to maximum likelihood parameter estimation, since

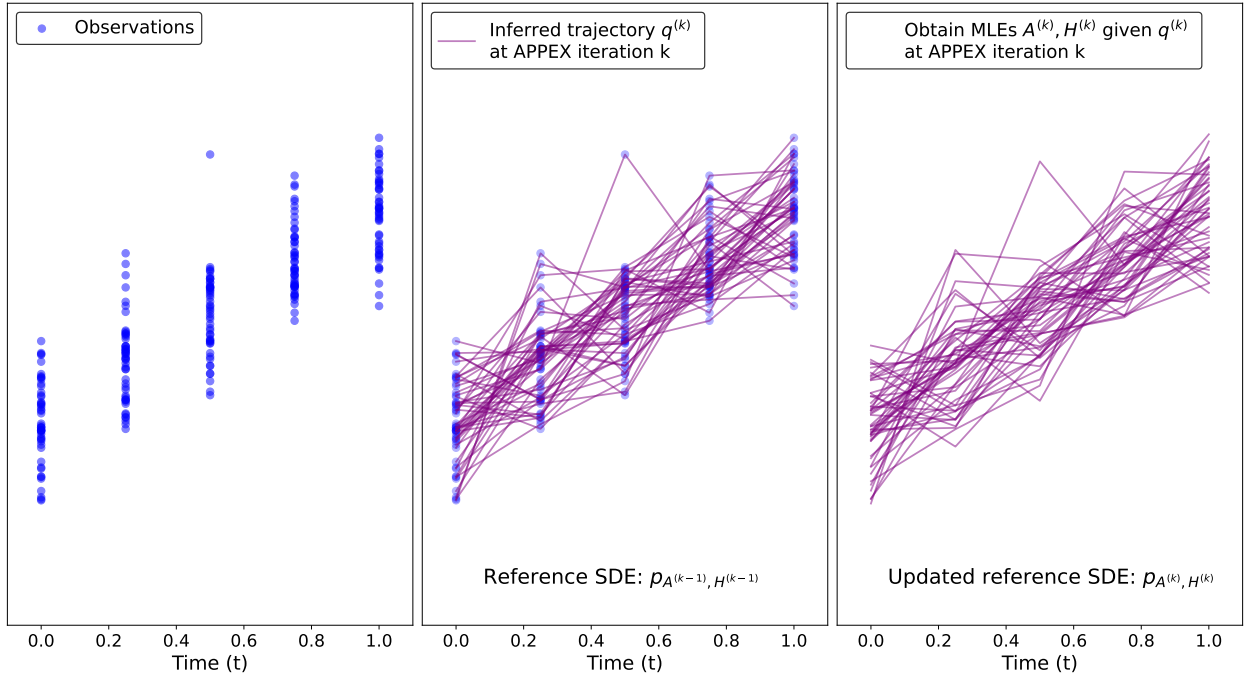


Figure 3: Visualization of our iterative parameter estimation algorithm APPEX. Given observed temporal marginals from an underlying SDE (left), APPEX alternates between trajectory inference (middle) and MLE parameter estimation (right) in order to find the SDE parameters that best represent the temporal marginal observations.

it amounts to determining the law on paths $p \in \mathcal{A}$ over linear additive noise SDEs, which best aligns with the law of the estimated trajectories q . Indeed, in the infinite-data limit, MLE is equivalent to minimizing relative entropy, i.e. KL divergence [Aka98, Whi82]. At the population level, an iteration entails the updates:

$$q^{(k)} = \arg \min_{q \in \mathcal{D}} D_{KL}(q \| p_{A^{(k-1)}, H^{(k-1)}}) \quad (24)$$

$$A^{(k)} = \arg \min_{A \in \mathbb{R}^{d \times d}} D_{KL}(q^{(k)} \| p_{A, H^{(k-1)}}) \quad (25)$$

$$H^{(k)} = \arg \min_{H \in S_{\geq 0}^d} D_{KL}(q^{(k)} \| p_{A^{(k)}, H}). \quad (26)$$

In iteration k , we start by using the SDE parameters estimated from the previous iteration to define a reference SDE $p_{A^{(k-1)}, H^{(k-1)}} \in \mathcal{A}$. Using this reference SDE and the set of observed temporal marginals, we perform trajectory inference (24) (see middle plot of Figure 3). This problem is equivalent to a Schrödinger Bridge problem [VTLL21, BHCK23], which seeks the path distribution $q^{(k)} \in \mathcal{D}$ that minimizes relative entropy to the reference SDE, while satisfying the marginal constraints (22). After trajectory inference, we perform a two-step maximum likelihood estimation, in order to estimate the drift and diffusion. This in turn updates the law of the reference SDE $p_{A^{(k)}, H^{(k)}} \in \mathcal{A}$ for trajectory inference in the next iteration.

We note that this procedure can easily be adapted to a general additive noise SDE (1), provided that a corresponding maximum likelihood estimator is used for the nonlinear drift function $b^{(k)}(X_t)$, in place of $A^{(k)}$, in the drift update step (25). We show in Corollary 8.19 of the Appendix that the structure of the closed form diffusion MLE is unchanged for general additive noise SDEs.

Previous works [Zha24, SBB24b, VTLL21] implement similar iterative schemes, which alternate between trajectory inference and MLE parameter estimation. In contrast to our method, each of these works assumes that the diffusion of the process is known, and hence invariant across iterations. One theoretical reason for this assumption is to ensure finite KL divergence between the estimated trajectories and estimated SDEs for all iterations [VTLL21]. Given continuously observed marginals of a d -dimensional process, the KL divergence

between two laws on paths q, p is taken over the path space $\Omega = C([0, T], \mathbb{R}^d)$, such that

$$D_{KL}(q\|p) = \int_{\Omega} \log \left(\frac{dq}{dp}(\omega) \right) dq(\omega).$$

Thus, $D_{KL}(q\|p)$ will only be finite between two laws on paths if we can define the Radon-Nikodym derivative $\frac{dq}{dp}$ over path space Ω . By Girsanov's theorem, this is only ensured when both processes share the same diffusion [SBB24b, VTLL21]. However, if we only consider measurements from a finite number of observed marginals, the KL divergence of the discretized processes q^N, p^N over the path space projected on the N measurement times, $\Sigma_{\mathcal{D}} = C(\{t_i\}_{i=0}^{N-1}, \mathbb{R}^d)$, can be decomposed as follows, see [BCDMN19]:

$$D_{KL}(q^N\|p^N) = \sum_{i=0}^{N-2} D_{KL}(q_{i,i+1}\|p_{i,i+1}) - \sum_{i=1}^{N-2} D_{KL}(q_i\|p_i), \quad (27)$$

where $p_{i,i+1}, q_{i,i+1}$ are the joint probability measures of q, p , restricted to times t_i and t_{i+1} , and similarly q_i, p_i are the marginals of q, p at time t_i . We note that $D_{KL}(q_i\|p_i) \leq D_{KL}(q_{i,i+1}\|p_{i,i+1})$ holds by the data-processing inequality. Hence, $D_{KL}(q^N\|p^N)$ will be finite as long as $D_{KL}(q_{i,i+1}\|p_{i,i+1}) = \int_{\mathbb{R}^d \times \mathbb{R}^d} \log \left(\frac{dq_{i,i+1}}{dp_{i,i+1}}(x) \right) q_{i,i+1}(x) dx < \infty$ for each $i = 0, \dots, N-1$. In particular, if p and q are the laws of two different drift-diffusion SDEs with distinct non-degenerate diffusions, then the KL divergence $D_{KL}(q^N\|p^N)$ over the discretized path space $\Sigma_{\mathcal{D}}$ will be finite. Since we consider a setting with a finite number of temporal marginal observations in this work, we may consider laws on paths discretized over these observations. This allows us to both consider diffusions which are not known in advance, and improve our diffusion estimates with respect to KL divergence after each iteration.

5.1 Trajectory inference via anisotropic entropy-regularized optimal transport

To begin each iteration of APPEX, we need to infer trajectories, given the set of temporal marginals $\{p_i\}_{i=0}^{N-1}$, and a reference SDE, $p_{A^{(k-1)}, H^{k-1}} \in \mathcal{A}$. As previously discussed, this is equivalent to the Schrödinger Bridge problem (24), which may be solved via entropy-regularized optimal transport (EOT). Given two marginals μ, ν , the solution to the standard EOT problem of transporting probability measure μ to ν with entropic regularization $\epsilon > 0$ and cost $c(x, y) = \|y - x\|^2/2$ is

$$\pi^* = \arg \min_{\pi \in \Pi(\mu, \nu)} \int c(x, y) d\pi(x, y) + \epsilon^2 D_{KL}(\pi\|\mu \otimes \nu) = \arg \min_{\pi \in \Pi(\mu, \nu)} \int \frac{\|y - x\|^2}{2\epsilon^2} d\pi(x, y) + D_{KL}(\pi\|\mu \otimes \nu). \quad (28)$$

Furthermore, it is easy to see from the dual formulation (see (53) in the Appendix) that $\pi^* \in \Pi(\mu, \nu)$ is the joint distribution with marginals μ, ν , which minimizes relative entropy with respect to the reference measure $dK(x, y) = K(x, y)d\mu(x)d\nu(y)$ with density $K(x, y) \propto e^{\frac{c(x, y)}{\epsilon^2}} \propto e^{-\frac{\|y-x\|^2}{2\epsilon^2}}$ [PC⁺19, Zha24]:

$$\pi^* = \text{Proj}_{\Pi(\mu, \nu)}^{KL}(\mathcal{K}) = \arg \min_{\pi \in \Pi(\mu, \nu)} D_{KL}(\pi\|\mathcal{K}). \quad (29)$$

Remark 5.1 (Applying EOT for SDE trajectory inference). *In the standard ϵ -regularized OT problem (28), $K \sim \mathcal{N}(x, \epsilon^2 I_d)$ is an isotropic Gaussian kernel. As noted in [LZKS21], this implies that entropy regularized OT can be leveraged for trajectory inference from observed marginals, given a reference SDE. For example, to find the discretized law on paths $\pi^* \in \Pi(\mu, \nu)$ satisfying $P(X_t = \mu, X_{t+\Delta t} = \nu)$, which minimizes relative entropy to the law of a pure diffusion process $dX_t = \sigma dW_t$, one should set the entropic regularization $\epsilon^2 = \sigma^2 \Delta t$. Indeed, this would correspond to minimizing the KL divergence to $K(x, y) = e^{-\frac{\|y-x\|^2}{2\sigma^2 \Delta t}} \sim \mathcal{N}(x, \sigma^2 \Delta t)$, which is the transition kernel of the reference SDE. Similarly, as done in [Zha24], one can perform trajectory inference given an Ornstein-Uhlenbeck reference SDE $dX_t = -AX_t dt + \sigma dW_t$ by approximating the transition distribution $X_{t+\Delta t}|x_t$ via $K(x, y) = e^{-\frac{\|y - e^{A\Delta t}x\|^2}{2\sigma^2 \Delta t}}$. This would correspond to reweighting the squared Euclidean cost with the drift matrix A , such that $c(x, y) = \|y - e^{A\Delta t}x\|^2/2$, and applying standard entropy regularized OT with $\epsilon^2 = \sigma^2 \Delta t$.*

However, the standard EOT problem (28) only considers a scalar regularization parameter ϵ , which means that it can only directly model reference SDEs with isotropic diffusion. To generalize trajectory inference for SDEs with anisotropic diffusion, we formalize ‘‘anisotropic entropy-regularized optimal transport’’ (AEOT),

by considering transition kernels K with custom mean and covariance, e.g. parameterizing K with A and $H = GG^\top$ rather than the scalar $\epsilon^2 > 0$. Indeed, we can consider more general Gaussian transition kernels, $K_\theta(x, y) = \exp\left(\frac{(y - \mu(x, \theta))^\top \Sigma(\theta)^{-1} (y - \mu(x, \theta))}{2}\right)$, in order to model a transition $y|x \sim \mathcal{N}(\mu(x, \theta), \Sigma(\theta))$, whose covariance $\Sigma(\theta)$ is possibly anisotropic. Under this formulation, the cost is given by the inner product $c_\theta(x, y) = \frac{(y - \mu(x, \theta))^\top \Sigma(\theta)^{-1} (y - \mu(x, \theta))}{2}$. Trajectory inference would amount to solving the AEOT problem:

$$\pi^* = \arg \min_{\pi \in \Pi(\mu, \nu)} \int \frac{(y - \mu(x, \theta))^\top \Sigma(\theta)^{-1} (y - \mu(x, \theta))}{2} d\pi(x, y) + D_{KL}(\pi \| \mu \otimes \nu), \quad (30)$$

where the entropic regularization is captured in the matrix $\Sigma(\theta)$ and function $\mu(x, \theta)$. Just as in the standard EOT problem, the AEOT solution π^* can be obtained by Sinkhorn's algorithm.

Proposition 8.18 in the Appendix shows that the solution to the trajectory inference step (24) is the joint distribution given by the Markov concatenation of couplings (see Definition 8.17 in the Appendix)

$$\pi^* = \pi_{0,1} \circ \dots \circ \pi_{N-2, N-1},$$

where $\pi_{i, i+1}$ is the AEOT solution (30) with marginals $\mu = p_i, \nu = p_{i+1}$ and transition kernel

$$K_{A, H}^i(x, y) \propto \exp\left(-\frac{1}{2}(y - e^{A(t_{i+1}-t_i)}x)^\top (\Sigma_i)^{-1} (y - e^{A(t_{i+1}-t_i)}x)\right) \quad (31)$$

such that $\Sigma_i = \int_{t_i}^{t_{i+1}} e^{A(t_{i+1}-s)} H e^{A^\top(t_{i+1}-s)} ds$. The reference transition $X_{t_{i+1}}|X_{t_i} \sim \mathcal{N}(e^{A(t_{i+1}-t_i)}X_{t_i}, \Sigma_i)$ can be estimated via the first order approximation $\mathcal{N}(X_t + AX_t(t_{i+1} - t_i), H(t_{i+1} - t_i))$.

Remark 5.2 (Application to empirical marginals). *Proposition 8.18 applies in the case where one observes the exact temporal marginals p_i . However, in practice we observe empirical measures \hat{p}_i which, in the limit of infinite data, converge almost surely in distribution to p_i . It is for these empirical measures \hat{p}_i which we actually compute the estimated couplings $\hat{\pi}_{i, i+1}$ in practice. This corresponds to numerically estimating the AEOT solution*

$$\hat{\pi}_{i, i+1} = \arg \min_{\pi \in \Pi(\hat{p}_i, \hat{p}_{i+1})} \int \frac{(y - \mu(x, \theta))^\top \Sigma(\theta)^{-1} (y - \mu(x, \theta))}{2} d\pi(x, y) + D_{KL}(\pi \| \hat{p}_i \otimes \hat{p}_{i+1}). \quad (32)$$

By the main theorem in [GNB22], it holds that $\hat{\pi}_{i, i+1}$ converges in distribution almost surely to the minimizer of (30) with $\mu = p_i$ and $\nu = p_{i+1}$ as the number of samples goes to infinity for each time i and $i + 1$. Combining this with the previous proposition, we see that estimating (32) for each pair of times i and $i + 1$ is asymptotically equivalent to the KL minimization step in (24).

We also note that (32) is practically solved using Sinkhorn's algorithm with empirical marginals \hat{p}_i, \hat{p}_{i+1} and the discretized transition kernel K_θ of the reference SDE. For example, if we have M samples per empirical marginal, then $\hat{p}_i \sim \text{Unif}(x_{t_i}^{(j)} : j = 1, \dots, M)$ and $\hat{p}_{i+1} \sim \text{Unif}(x_{t_{i+1}}^{(j)} : j = 1, \dots, M)$ would both be discrete uniform distributions over their samples, and $K_\theta \in \mathbb{R}^{M \times M}$ would be a square matrix, such that entry $K_{\theta_{j,k}}$ is obtained by applying the given transition kernel on the data points $x_{t_i}^{(j)}$ and $x_{t_{i+1}}^{(k)}$.

5.2 Parameter estimation via MLE

To optimize objectives (25) and (26) for each iteration of APPEX, we require maximum likelihood estimators for the SDE parameters in the setting of multiple observed trajectories from $[0, T]$. We derive closed-form maximum likelihood estimators for the linear additive noise SDE from Equation 2, given multiple trajectories. In the context of iteration k of APPEX, these are the trajectories sampled from the law on paths $q^{(k)}$ obtained from the trajectory inference step.

Proposition 5.3 (MLE estimators for drift and diffusion of SDE (2) from multiple trajectories). *Given M trajectories over N equally spaced times: $\{X_{i\Delta t}^{(j)} : i = 0, \dots, N - 1, j = 0, \dots, M - 1\}$ sampled from the linear additive noise SDE (2), the maximum likelihood solution for linear drift is approximated by*

$$\hat{A} = \frac{1}{\Delta t} \left(\sum_{i=0}^{N-2} \sum_{j=0}^{M-1} (\Delta X_i^{(j)}) X_i^{(j)\top} \right) \left(\sum_{i=0}^{N-2} \sum_{j=0}^{M-1} X_i^{(j)} X_i^{(j)\top} \right)^{-1} \quad (33)$$

$$\xrightarrow{M \rightarrow \infty} \frac{1}{\Delta t} \left(\sum_{i=0}^{N-2} \mathbb{E}_{p_{i, i+1}} [(\Delta X_i) X_i^\top] \right) \left(\sum_{i=0}^{N-1} \mathbb{E}_{p_i} [X_i X_i^\top] \right)^{-1}, \quad (34)$$

where $p_{i,i+1}$ is the joint measure over X_{t_i} and $X_{t_{i+1}}$. Similarly, the maximum likelihood solution for diffusion is approximated by

$$\hat{H} = \frac{1}{MT} \sum_{i=0}^{N-2} \sum_{j=0}^{M-1} \left(\Delta X_i^{(j)} - AX_i^{(j)} \Delta t \right) \left(\Delta X_i^{(j)} - AX_i^{(j)} \Delta t \right)^\top \quad (35)$$

$$\xrightarrow{M \rightarrow \infty} \frac{1}{T} \sum_{i=0}^{N-2} \mathbb{E}_{p_{i,i+1}} [(\Delta X_i - AX_i \Delta t) (\Delta X_i - AX_i \Delta t)^\top] \quad (36)$$

Proof. See Section 8.6 of the Appendix. We note that estimators \hat{A} and \hat{H} were derived using the discretized transition kernel, $X_{i+1}|X_i \sim \mathcal{N}(X_i + AX_i \Delta t, H \Delta t)$. We derive the maximum likelihood estimators with the exact transition kernel $X_{i+1}|X_i \sim \mathcal{N}(e^{A \Delta t} X_i, H \Delta t)$ in the one dimensional case in Section 8.6. \square

Remark 5.4. Note that the MLE estimator for drift A does not depend on the diffusion H , but the MLE estimator for H depends on A . Therefore, we estimate drift first in each iteration of APPEX.

5.3 The APPEX algorithm

APPEX has two main subprocedures. We first perform a trajectory inference step (24), via anisotropic entropy-regularized optimal transport (AEOT), our adaptation of EOT for general additive noise SDEs. This step is outlined in line 6 of Algorithm 1. We then perform two maximum likelihood parameter estimation steps (25)-(26), where we have derived approximate MLE solutions for linear drift and additive diffusion in Proposition 5.3. These steps are outlined in lines 9 and 10 of Algorithm 1. Because these subprocedures are optimal with respect to minimizing KL divergence, we can show that APPEX's estimates will improve with each iteration.

Lemma 5.5. Suppose that A and H are the true drift and diffusion parameters of a linear additive noise SDE with temporal marginals p_0, \dots, p_{N-1} . Let $q^{(k)} \in \mathcal{D}$ be the law of the estimated trajectories at iteration k of APPEX, and $p_{A^k, H^k} \in \mathcal{A}$ be the law of the law of the estimated linear additive noise SDE, such that $A^0 \in \mathbb{R}^{d \times d}$ and $H^0 \in S_{\geq 0}^d$. Then, the relative entropy between the estimated law of the trajectories and the law of the estimated linear additive noise SDE is decreasing with each iteration:

$$D_{KL}(q^{(k+1)} \| p_{A^{k+1}, H^{k+1}}) \leq D_{KL}(q^{(k)} \| p_{A^k, H^k}) \quad \forall k \geq 0.$$

Furthermore, if p_0 is not auto-rotationally invariant, then as the number of observed marginals $N \rightarrow \infty$, the relative entropy between the estimated law of the trajectories and the law of the estimated SDE is uniquely minimized by the underlying SDE $p_{A,H}$:

$$\inf_{q \in \mathcal{D}, p \in \mathcal{A}} D_{KL}(q \| p) = 0 \iff q = p = p_{A,H}$$

Proof. Proposition 8.18 shows that $q^{(k+1)} \in \mathcal{D}$ minimizes relative entropy to p_{A^k, H^k} . Similarly, any MLE solution $p_{A^{(k+1)}, H^{(k+1)}}$ minimizes relative entropy to $q^{(k+1)}$. In particular, Proposition 5.3 approximates the MLE parameters $A^{k+1} \in \mathbb{R}^{d \times d}$ and $H^{(k+1)} \in S_{\geq 0}^d$. By construction of the iterative scheme, we have that

$$D_{KL}(q^{(k+1)} \| p_{A^{(k+1)}, H^{(k+1)}}) \leq D_{KL}(q^{(k+1)} \| p_{A^{(k+1)}, H^{(k)}}) \leq D_{KL}(q^{((k+1))} \| p_{A^{(k)}, H^{(k)}}) \leq D_{KL}(q^{(k)} \| p_{A^{(k)}, H^{(k)}}),$$

which proves the first claim of the lemma. Furthermore, if X_0 is not auto-rotationally invariant, then by our identifiability result (Theorem 4.3), as we increase the number of temporal marginals $N \rightarrow \infty$, $p_{A,H}$ is the law of the unique linear additive noise SDE, which obey the marginal constraints p_0, \dots, p_{N-1} . Equivalently, we have $\mathcal{A} \cap \mathcal{D} = \{p_{A,H}\}$ and

$$\inf_{q \in \mathcal{D}, p \in \mathcal{A}} D_{KL}(q \| p) = 0 \iff q = p = p_{A,H},$$

\square

Since the relative entropy $D_{KL}(q^{(k)} \| p_{A^{(k)}, H^{(k)}})$ is decreasing for successive iterations k , this implies that the drift and diffusion estimates $A^{(k)}, H^{(k)}$ increasingly fit the data with each iteration. In this sense, our method is always approaching the true solution, which is unique, provided that it is given an appropriate initial distribution and sufficient observations.

Algorithm 1 Parameter estimation for an additive noise SDE from temporal marginals with APPEX

```
1: Input: Observed marginals  $\hat{p}_i, i = 0, \dots, N - 1$ , number of iterations  $K, \Delta t$ 
2: Result: Estimated drift function  $\hat{b}$  and additive noise  $\hat{H}$ 
3: Initialize:  $\hat{b} \leftarrow 0, H \leftarrow \sigma^2 \mathbf{I}_d, k \leftarrow 0$ 
4: while  $k < K$  do
5:   for  $i = 1, \dots, N$  do
6:      $\hat{\pi}_{i,i+1} \leftarrow \text{Anisotropic-Entropy-Regularized-Optimal-Transport}(\hat{b}, \hat{H}, \hat{p}_{i-1}, \hat{p}_i, \Delta t)$ 
7:   end for
8:   Sample-Trajectories  $\leftarrow \hat{\pi}_{N-1,N} \circ \dots \circ \hat{\pi}_{1,2}(p_0)$ 
9:    $\hat{b} \leftarrow \text{MLEfit}(\text{Sample-Trajectories})$ 
10:   $\hat{H} \leftarrow \text{MLEfit}(\text{Sample-Trajectories}, \hat{b})$ 
11:   $k \leftarrow k + 1$ 
12: end while
13:  $\mathcal{G} \leftarrow \text{Estimate-Causal-Graph}(\hat{b}, \hat{H}, \epsilon)$ 
```

Remark 5.6 (Application to causal discovery). *As proven in Lemma 4.5 and visualized in Figure 1, the causal graph can be derived from the SDE parameters. For nonlinear drift $b(X_t)$, we include the edge $i \rightarrow j$ if the j th component of the drift, b_j , is a function of $X^{(i)}$. For linear drift one may simply examine $A_{j,i}$. For multi-edges, one can check $H_{i,j}$ to determine whether there is an unobserved confounder causing $X^{(i)}$ and $X^{(j)}$. We therefore include a causal discovery step in line 13 of Algorithm 1. We acknowledge that many causal algorithms and independence tests are applicable, and leave the implementation as general as possible.*

6 Experiments

In this section, we evaluate the performance of our parameter estimation method APPEX on simulated data. We first demonstrate that the non-identifiable examples from Section 3 can be correctly identified by APPEX if the initial marginal X_0 is not auto-rotationally invariant. We then show that combining our initialization with our parameter estimation method successfully learns arbitrary dynamical systems modelled with a linear additive noise SDE by testing it on randomly generated SDEs across a range of dimensions. We conclude this section with several causal graph recovery experiments. An empirical experiment for consistency is also provided in Appendix 9.1, which shows that over a broad class of random experiments, APPEX’s estimates for both drift and diffusion converge to the true SDE parameters.

6.1 Experimental setup

For each experiment, we simulate data for linear additive noise SDEs using Euler-Maruyama discretization with $dt_{EM} = 0.01$, such that we generate $M = 500$ trajectories, each observed across 100 time steps. Each d -dimensional trajectory is initialized with $p_0 \sim \text{Unif}\{x_i\}_{i=1}^d$ where $\{x_i\}_{i=1}^d$ are randomly sampled linearly independent vectors with each entry having a magnitude between 2 and 10. It follows from Proposition 8.11 and Theorem 4.3, that this initial distribution ensures that parameter estimation is feasible.

To model the setting where we only observe temporal marginals, we subsample at the rate $dt = 0.05$ to produce $N = 20$ marginals with $M = 500$ observations per time. To perform parameter estimation, we use 30 iterations of our APPEX algorithm, such that the initial reference SDE is an isotropic Brownian motion $dX_t = \sigma dW_t$, even when the true process has anisotropic noise. To model the realistic setting where diffusion is not precisely known, we assume that the initial guess of the diffusion’s trace is within an order of magnitude of the ground truth trace $\text{tr}(H)$. Specifically, we initialize $A^{(0)} = 0, H^{(0)} = \sigma^2 \mathbf{I}_d$ s.t. $\sigma^2 \sim \text{tr}(H) 10^{\text{Unif}(-1,1)}$. Because the first reference SDE is σdW_t , we note that the first iteration of APPEX is equivalent to inferring trajectories using the Waddington-OT (WOT) method from [SST+19], based on standard regularized OT (28) with $\epsilon^2 = \sigma^2 \Delta t$, followed by MLE parameter estimation. APPEX and WOT are distinguished by the fact that APPEX benefits from further iterations, and allows the reference SDE to have anisotropic diffusion and non-zero drift. For each iteration of APPEX, we use Sinkhorn’s algorithm to solve the anisotropic entropy-regularized optimal transport problem for trajectory inference, and we use the closed form MLE solutions from Proposition (5.3). Due to time complexity and numerical stability, we use linearized discretizations for the Gaussian transition kernels (unless $d = 1$).

6.2 Revisiting previously non-identifiable SDEs

We perform parameter estimation on the three pairs of SDEs from Section 4. 10 replicates of each experiment were performed, such that each replicate featured data from different valid p_0 initializations and different initial diffusivities σ^2 . To measure performance, we track the mean absolute error (MAE), plotted in Figure 4, between the true drift/diffusion parameters and their estimates.

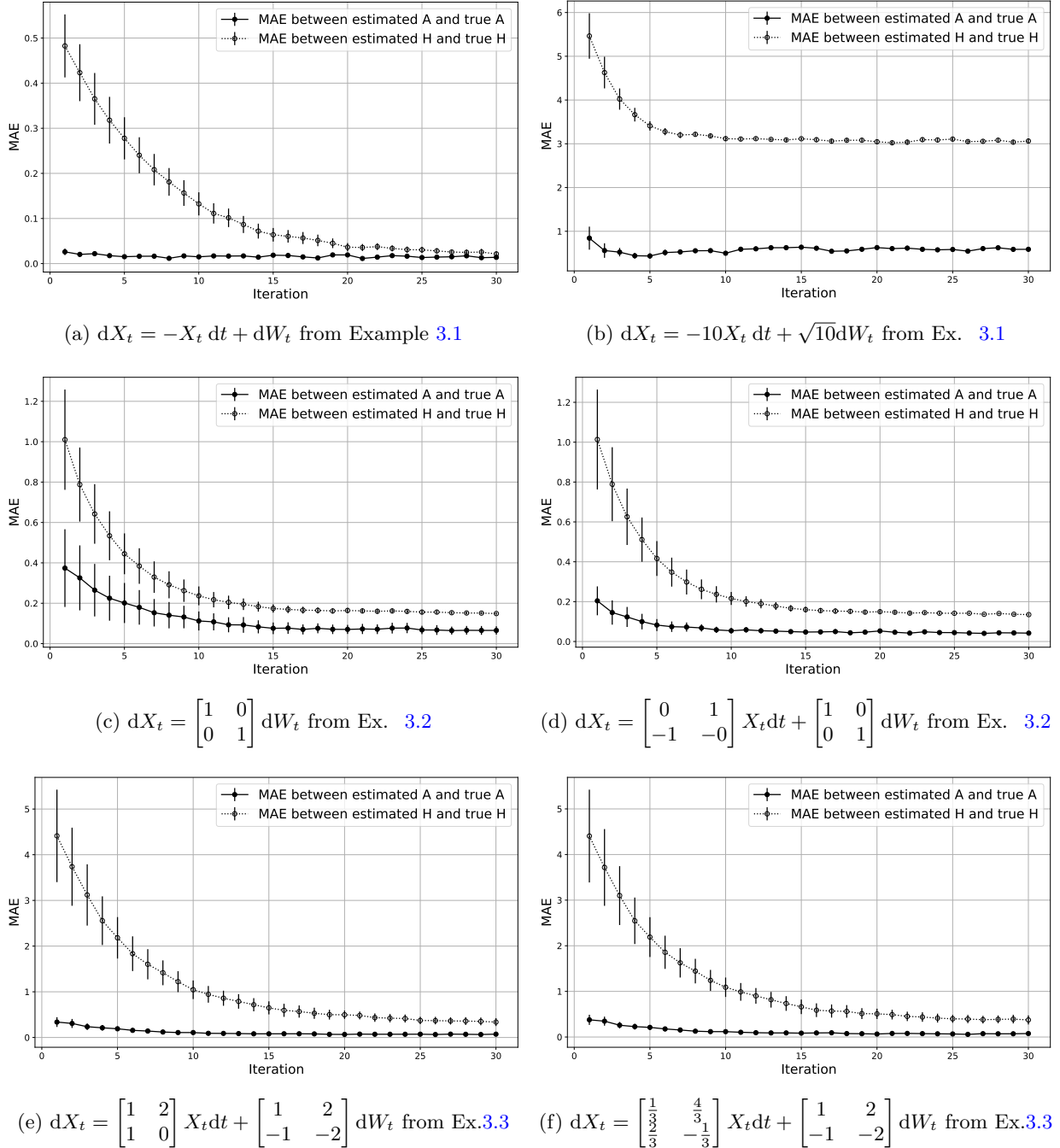


Figure 4: The mean absolute error for estimates of A and H using APPEX is shown per iteration for all three pairs of SDEs from Section (4)

The results demonstrate that in each example, APPEX is able to estimate both drift and diffusion by iteratively improving upon both estimates. In each experiment, we observe decreasing MAEs for both SDE parameters as the number of iterations increases. The worst performance was observed for the SDE $dX_t = -10X_t dt + \sqrt{10}dW_t$, whose significantly higher noise scale made inference more difficult, particularly

for the diffusion, which APPEX consistently estimated around $H = 7$ rather than $H = 10$. We note that even though degenerate diffusions can result in infinite KL divergence with respect to a misspecified reference SDE, we observe that APPEX can estimate degenerate diffusions, such as in Example 3.3.

6.3 Higher dimensional random matrices

We now test APPEX on a broad range of higher dimensional random linear additive noise SDEs. For each dimension $d = 3, \dots, 10$, we generate 10 random SDEs. To create each drift matrix A , we randomly sample each of its d^2 entries from $\text{Unif}(-5, 5)$. To ensure that the values do not diverge, we verify that the maximal real part of the eigenvalues of A is less than 1. This allows us to consider process beyond OU processes, while obeying reasonable growth conditions in practice. To create each diffusion G , we randomly initialize each of its d^2 entries via $\text{Unif}(-1, 1)$ and then set $H = GG^\top$. For numerical stability, we perform Sinkhorn on the logarithmic scale for this experiment.

Table 1: Mean absolute error (MAE) of estimated drift and diffusion for dimensions 3-10. Our method (APPEX) consistently outperforms (bold) the previous method (WOT).

Dimension	A Estimation		GG^\top Estimation	
	WOT	APPEX	WOT	APPEX
3	0.351 ± 0.04	0.237 ± 0.04	0.793 ± 0.205	0.147 ± 0.030
4	0.730 ± 0.067	0.328 ± 0.041	1.549 ± 0.439	0.415 ± 0.070
5	0.912 ± 0.060	0.602 ± 0.195	2.174 ± 0.702	0.362 ± 0.039
6	1.43 ± 0.170	0.358 ± 0.020	18.010 ± 8.636	0.256 ± 0.046
7	1.480 ± 0.132	0.360 ± 0.015	6.807 ± 1.724	0.345 ± 0.037
8	1.862 ± 0.137	0.460 ± 0.015	5.472 ± 1.266	0.359 ± 0.019
9	1.803 ± 0.222	0.487 ± 0.016	8.134 ± 3.024	0.454 ± 0.122
10	1.670 ± 0.241	0.439 ± 0.019	35.122 ± 28.529	0.317 ± 0.025

Table 2: Correlation between estimated and true drift and diffusion for dimensions 3-10. Our method (APPEX) consistently outperforms (bold) the previous method (WOT).

Dimension	A Estimation		GG^\top Estimation	
	WOT	APPEX	WOT	APPEX
3	0.996 ± 0.001	0.998 ± 0.001	0.837 ± 0.048	0.985 ± 0.005
4	0.943 ± 0.015	0.987 ± 0.005	0.729 ± 0.039	0.865 ± 0.031
5	0.921 ± 0.016	0.952 ± 0.030	0.728 ± 0.040	0.909 ± 0.018
6	0.794 ± 0.040	0.986 ± 0.001	0.530 ± 0.056	0.961 ± 0.007
7	0.792 ± 0.029	0.988 ± 0.001	0.595 ± 0.037	0.946 ± 0.012
8	0.699 ± 0.035	0.981 ± 0.002	0.611 ± 0.042	0.949 ± 0.006
9	0.740 ± 0.033	0.978 ± 0.002	0.615 ± 0.025	0.919 ± 0.033
10	0.760 ± 0.049	0.983 ± 0.001	0.641 ± 0.041	0.960 ± 0.006

The results demonstrate that APPEX continues to estimate both SDE parameters robustly across all settings. Importantly, APPEX can handle arbitrary additive noise structures $H = GG^\top$, as evidenced by high correlations to the true diffusion and low MAE. This is significant because previous literature has focused on the setting of isotropic noise, but in practice, we expect noise structures to have off-diagonal entries due to shared noise from unobserved confounders, as well as unequal noise along the main diagonal. In contrast, although WOT estimates the drift somewhat decently, it is unable to estimate the diffusion accurately, particularly in higher dimensions, since it is constrained to isotropic noise in its reference SDE. Figure (5) shows how APPEX is able to re-orient incorrect diffusion priors to closely match the true diffusion of the underlying SDE.

6.4 Causal discovery

We conclude with experiments that demonstrate APPEX’s ability to recover the causal graph of the underlying dynamic system. We first consider causal discovery from systems without latent confounders, and then

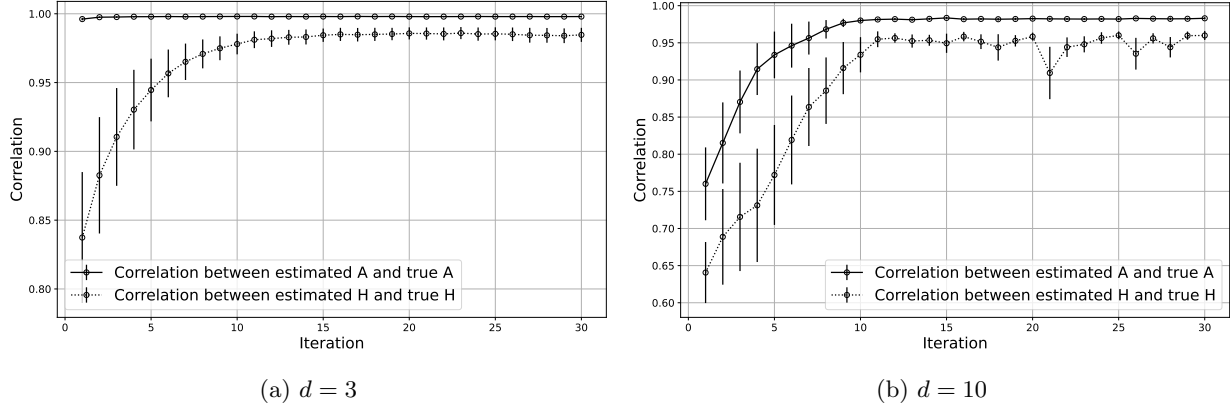


Figure 5: The correlation between the estimated and true SDE parameters is plotted per iteration across 10 random linear additive noise SDEs for dimensions 3 and 10

consider causal discovery from systems with latent pairwise confounders.

We evaluate APPEX using the default experimental settings laid out in Section 6.1 across randomly generated SDEs of dimension $d = 3, 5, 10$. In particular, we consider Erdős-Renyi graphs $G(d, p)$, such that each of the $d(d - 1)$ possible simple directed edges are included with probability p . As in Section 6.3, we ensure that the maximal eigenvalue of the randomly generated ground truth drift matrix is at most 1 to prevent unbounded growth. We will see that accurately estimating the diffusion is important for recovering the correct causal graph.

6.4.1 Causal discovery under causal sufficiency

Lemma 4.5 states that simple directed edges $e = i \rightarrow j \in E$ in the causal graph $\mathcal{G} = ([d], E, \tilde{E})$ are characterized by the condition $A_{j,i} \neq 0$. To simulate ground truth edges, we follow standard convention for simulating data for causal discovery, by simulating edge weights $A_{j,i}$ uniformly via $\text{Unif}(-5, 0.5) \cup \text{Unif}(0.5, 5)$ [Run21, RSW21]. We then determine the presence of edge $i \rightarrow j$, if in the estimated drift, $\hat{A}_{j,i} > \epsilon$ (corresponding to a positive edge weight) or $\hat{A}_{j,i} < -\epsilon$ (corresponding to a negative edge weight). We choose our threshold $\epsilon = 0.5$ according to the minimal edge weight magnitude from simulated construction.

To model the case where the observed system does not have any latent confounders, we set the diffusion G to be zero for all entries outside its main diagonal. Thus, the only edges in the causal graph \mathcal{G} are simple directed edges, attributed to the drift. Similarly to the experiment on higher dimensional random matrices, we set each of the d diagonal entries of G via $\text{Unif}(0, 1)$.

We measure performance according to the structural Hamming distance. In particular, a system’s causal graph consists of directed edges $i \rightarrow j$ with positive weights $A_{j,i} > 0$ ($\hat{A}_{j,i} > \epsilon$), directed edges $i \rightarrow j$ with negative weights $A_{j,i} < 0$ ($\hat{A}_{j,i} < -\epsilon$), and absence of edges $A_{j,i} = 0$ ($|\hat{A}_{j,i}| < \epsilon$). The structural Hamming distance adds 1 for every instance in which an edge is misclassified, and is defined by

$$d(\mathcal{G}(A), \mathcal{G}(\hat{A})) = \sum_{(i,j) \in [d] \times [d]} \mathbf{1} \left\{ \text{sgn}(A_{j,i}) \neq \text{sgn}(\hat{A}_{j,i}) \mathbf{1}_{|\hat{A}_{j,i}| > \epsilon} \right\}. \quad (37)$$

The mean structural Hamming distances of causal graphs estimated by WOT and APPEX, across various dimensions $d \in \{3, 5, 10\}$ and random edge probabilities $p \in \{0.1, 0.25, 0.5\}$, are given in Table 3. We also plot the true vs. estimated graphs by WOT and APPEX for two SDEs in Figure 6.

While WOT often struggles to learn the causal graph, due to drift estimates compensating for misspecified diffusion [Hua24], APPEX consistently recovers the causal graph, including cycles and v-structures. For example, the first row in Figure 6 demonstrates that APPEX recovers the system’s negative feedback structure, while WOT introduces additional cycles between variables to make sense of the data with poorly estimated diffusion. This highlights the fact that one must estimate diffusion accurately in order to recover an accurate causal representation of the system from the drift.

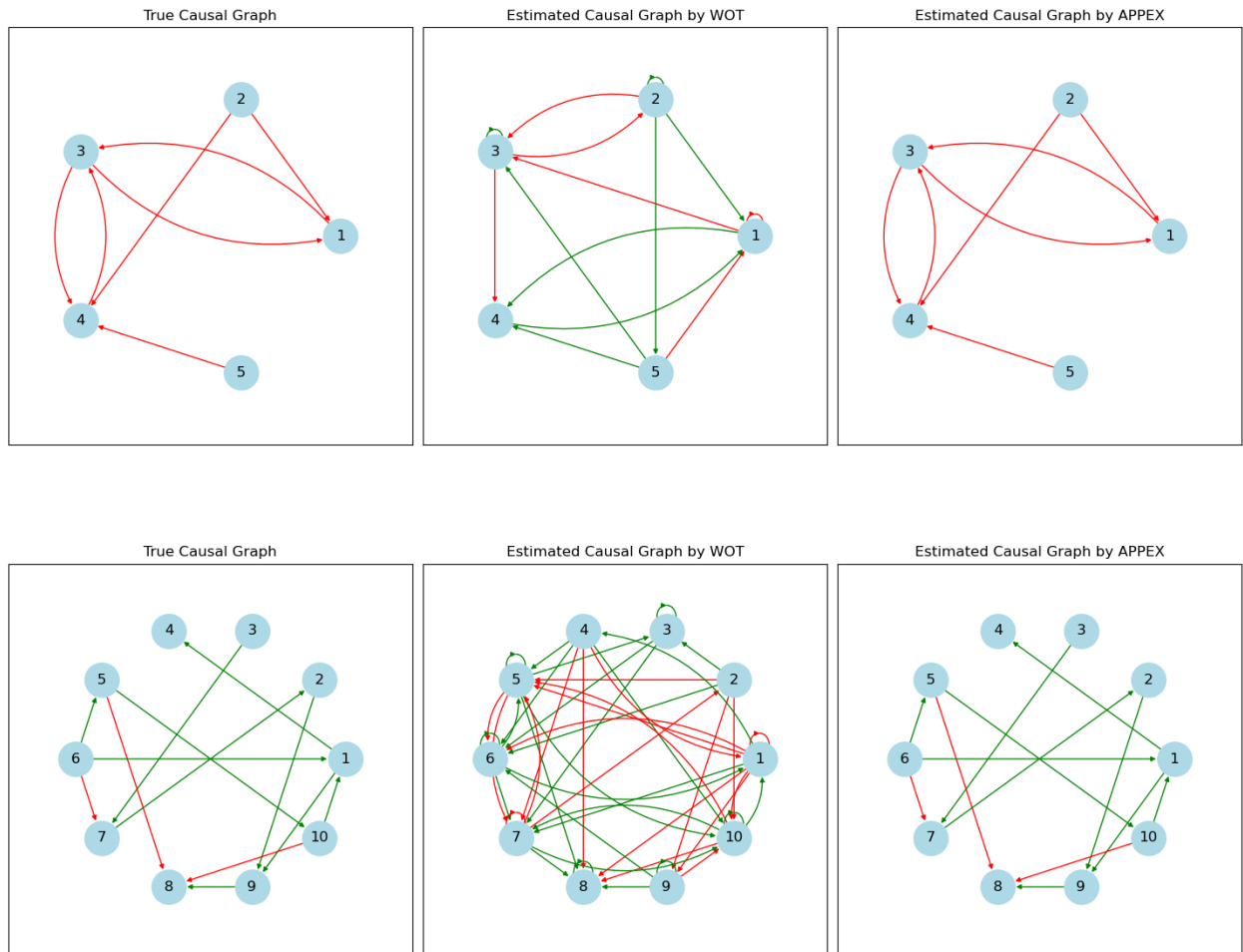


Figure 6: The true and estimated causal graphs by WOT and APPEX for two random SDEs of dimensions $d = 5, 10$ are illustrated. Red edges $i \rightarrow j$ represent negative edge weights, such that $X^{(i)}$ negatively regulates $X^{(j)}$. Green edges $i \rightarrow j$ represent positive edge weights, such that $X^{(i)}$ positively regulates $X^{(j)}$.

Table 3: Average Structural Hamming Distance (lower is better) with varying dimensions and random edge probabilities p . Our method (APPEX) consistently outperforms (bold) the previous method (WOT).

Dimension	$p = 0.1$		$p = 0.25$		$p = 0.5$	
	WOT	APPEX	WOT	APPEX	WOT	APPEX
3	0.40 ± 0.40	0.00 ± 0.00	1.80 ± 0.76	0.30 ± 0.30	1.40 ± 0.65	0.00 ± 0.00
5	3.80 ± 2.13	0.10 ± 0.10	3.56 ± 1.70	0.00 ± 0.00	4.40 ± 1.14	0.60 ± 0.22
10	38.30 ± 8.53	0.50 ± 0.40	48.60 ± 6.55	0.80 ± 0.39	37.4 ± 4.66	3.30 ± 0.70

6.4.2 Causal discovery with latent confounders

Lemma 4.5 also states that pairwise latent confounders, represented by bi-directed edges $\tilde{e} = i \leftrightarrow j$ in the causal graph $\mathcal{G} = ([d], E, \tilde{E})$ are characterized by the condition $H_{i,j} = H_{j,i} \neq 0$. Since we would also like to consider cycles formed by sets of simple directed edges, we consider the augmented causal $\tilde{\mathcal{G}} = (V, E)$ to more clearly model pairwise latent confounders, as done in [BM24]. Specifically, $\tilde{e} = i \leftrightarrow j \in \tilde{E}$ would correspond to the v-structure $i \leftarrow U_{i,j} \rightarrow j$ in the augmented graph $\tilde{\mathcal{G}}$, where $U_{i,j}$ is the unobserved pairwise confounder of $X^{(i)}$ and $X^{(j)}$.

To model the case where the observed system features pairwise latent confounders, we randomly select a subset of the columns of the diffusion G to feature precisely two nonzero entries, in two randomly chosen rows i, j . For simplicity, we initialize these entries $G_{i,k} = G_{j,k} = 1 \implies H_{i,j} = G_i \cdot G_j \geq 1$. We then determine the presence of the v-structure $i \leftarrow U_{i,j} \rightarrow j$ if in the estimated observational diffusion, $|\hat{H}_{i,j}| = |\hat{H}_{j,i}| > \epsilon$. We again pick our threshold to be $\epsilon = 0.5$.

We again measure performance according to the structural Hamming distance. For interpretability, we break the distance into two parts. We consider the Hamming distance based on the simple edges between observed variables, defined in (37), as well as the Hamming distance based on latent pairwise confounders, which adds 1 for every misclassified v-structure in the augmented graph:

$$d(\tilde{\mathcal{G}}(H), \tilde{\mathcal{G}}(\hat{H})) = \sum_{(i,j) \in [d] \times [d]: i \neq j} \mathbf{1} \left\{ (|H_{i,j}| > \epsilon \cap |\hat{H}_{i,j}| \leq \epsilon) \cup (|H_{i,j}| \leq \epsilon \cap |\hat{H}_{i,j}| > \epsilon) \right\}. \quad (38)$$

We evaluate APPEX and WOT across random SDEs of dimensions $d = 3, 5, 10$ with random edge probability $p = 0.25$ for simple edges. The number of pairwise latent confounders is chosen uniformly from $\{1, \dots, \lfloor \frac{2d}{3} \rfloor\}$. The results are summarized in Table 4. We also plot the true vs. estimated graphs by WOT and APPEX for two SDEs in Figure 7. We see that APPEX is able to recover both the simple edges and the latent pairwise confounders with high accuracy across dimensions. In contrast, WOT struggles to detect both, especially for higher dimensions. We note that in this setting with anisotropic diffusion, WOT’s initial diffusion reference is not only misspecified according to diagonal scaling, but further misspecifies the nonzero entries.

Table 4: Average Structural Hamming Distance for simple edges, and latent confounders (lower is better) with varying dimensions and random edge probability $p = 0.25$. Our method (APPEX) consistently outperforms (bold) the previous method (WOT).

Dimension	Hamming distance for simple edges		Hamming distance for latent confounders	
	WOT	APPEX	WOT	APPEX
3	1.20 ± 0.51	0.7 ± 0.40	1.00 ± 0.30	0.00 ± 0.00
5	4.80 ± 1.47	1.60 ± 0.87	3.50 ± 0.64	0.10 ± 0.10
10	38.00 ± 6.30	3.00 ± 0.77	23.80 ± 3.86	2.90 ± 1.39

7 Discussion

This work presents the first comprehensive approach for estimating both the drift and diffusion of SDEs from temporal marginals. We achieve this by proving that arbitrary time-homogeneous linear additive noise SDEs are identifiable from temporal marginals, provided that the initial distribution is not auto-rotationally invariant. This result eliminates the need for prior assumptions that drift or diffusion are known, as well as restrictive model simplifications, namely irrotational drift or isotropic diffusion, which were previously

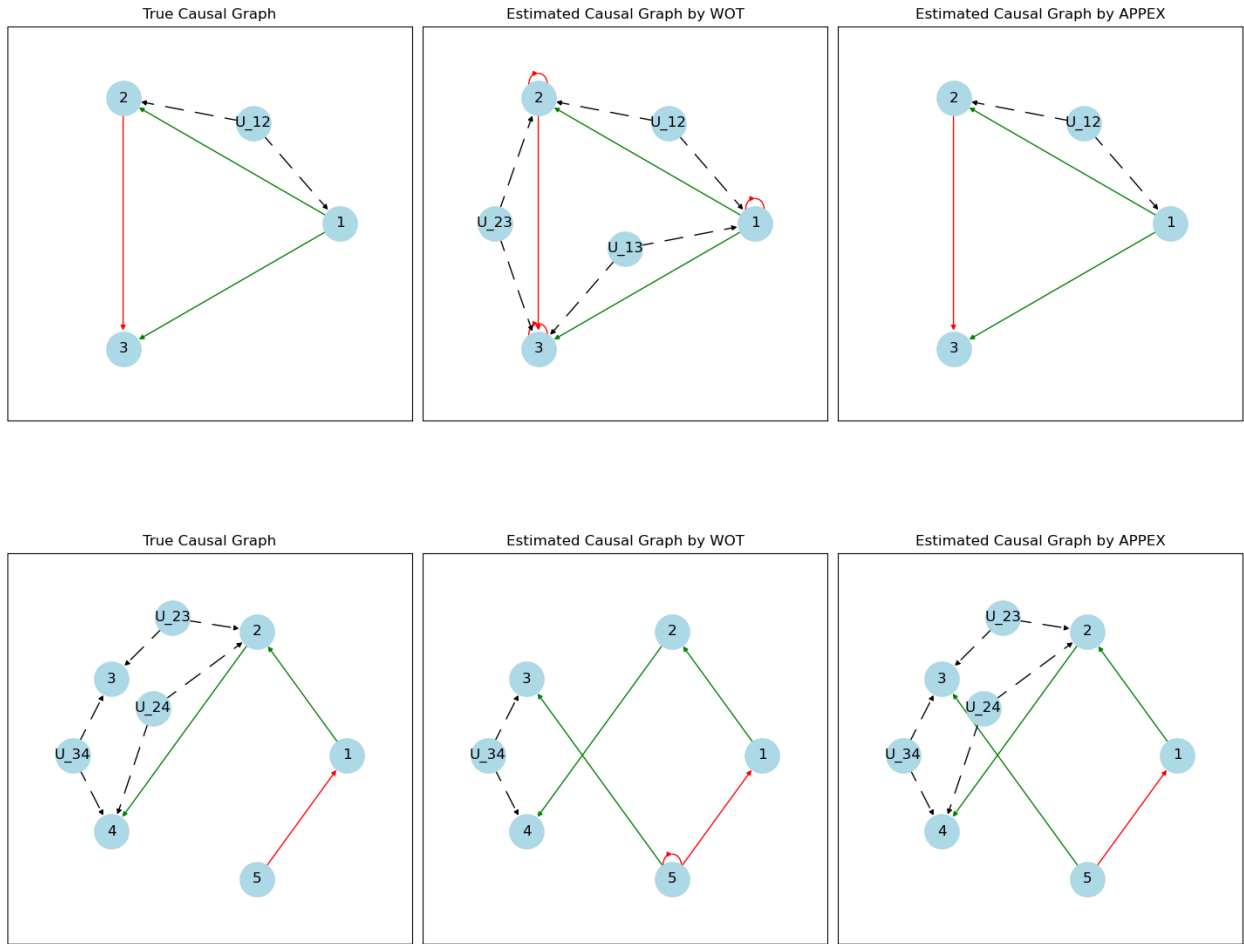


Figure 7: The true and estimated augmented causal graphs by WOT and APPEX for two random SDEs of dimensions $d = 3, 5$ are illustrated. Red edges $i \rightarrow j$ represent negative edge weights, such that $X^{(i)}$ negatively regulates $X^{(j)}$. Green edges $i \rightarrow j$ represent positive edge weights, such that $X^{(i)}$ positively regulates $X^{(j)}$. Dashed edges represent the effect of a latent confounder $U_{i,j}$ on observed variables i, j .

required to resolve non-identifiability. Additionally, we show that drift and diffusion identify the system’s causal graph. In sum, our theoretical contributions demonstrate that it is possible to precisely learn a process’s underlying dynamics—even in the presence of complex interactions, such as negative feedback loops and repressilator dynamics, or latent confounders—solely from temporal marginals. These insights have the potential to advance methods for trajectory inference and gene regulatory network (GRN) inference in single-cell biology.

In order to practically learn a process’ underlying dynamics from temporal marginals, we introduce the first method to simultaneously learn drift and diffusion from temporal marginals. To estimate arbitrary drift and additive noise, we apply anisotropic entropy-regularized optimal transport for anisotropic diffusions, and we pair this with maximum likelihood estimates of drift and diffusion. Our parameter estimation method, APPEX, then iterates towards the optimal parameter set by alternating between trajectory inference and parameter estimation. Given a non-auto-rotationally invariant initial distribution X_0 , we show that APPEX performs effectively across extensive experiments on simulated data from arbitrary linear additive noise SDEs. In particular, APPEX is able to recover the process’ drift, diffusion, and causal graph, in contrast to WOT, which is currently one of the most popular methods.

In terms of practical significance, we remark that non-auto-rotational invariance is satisfied by a large class of distributions. Hence, one can easily check the initial distribution, or perform an intervention if needed, to guarantee system identifiability from data generated by a linear additive noise SDE. Furthermore, we have proven the asymptotic optimality of each of APPEX’s subprocedures (Lemma 5.5): given a finite set of the process’ true marginals, APPEX improves its estimates with each iteration. Our experiments in the finite data setting (500 samples per temporal marginal) further motivate its practical use. Unlike WOT, APPEX accurately estimates drift, diffusion, and causal structure across hundreds of randomly generated SDEs between dimensions 3 to 10. APPEX therefore offers significant inference capability and flexibility compared to previous methods, since it can fully learn the dynamic system, without relying on prior knowledge. Even if a user is only interested in one parameter, APPEX offers the ability to estimate it, regardless of how the other parameter is initialized. This is particularly significant given that a misspecified diffusion typically leads to a misidentified drift, and vice-versa.

7.1 Limitations and future work

Although this paper presents several breakthroughs for the identification of SDEs from marginals, we acknowledge methodological limitations and opportunities for future work.

First, while we have proved that identifiability holds when the initial distribution X_0 is not auto-rotationally invariant, we have not yet studied the relative effectiveness of different initial distributions for parameter estimation. This could be an interesting area for further exploration, since the initial distribution may, at times, be controllable.

Second, our identifiability result is restricted to time homogeneous linear additive noise SDEs. Although this is a popular model for real-world processes, including the processes modeled by GRNs [RCM⁺24, Zha24], it would be beneficial to characterize identifiability conditions under more general models, in order to increase the practicality of our theory and methods. We note that characterizing identifiability will be particularly challenging for non-additive noise models, where the noise depends on the process X_t . For example, the same marginal observations can be explained by a nonlinear additive noise SDE and a linear multiplicative noise SDE [CHS22]. Our causal discovery results in Section 4.2 are also limited to additive noise. For this reason, it may be easier to consider identifiability for parametric families of nonlinear drift under the additive noise model. Similarly, we note that it should be straightforward to extend experimental evaluation of APPEX to SDEs with nonlinear drift. Indeed, although the MLEs may not have a closed form solution, optimizers like BFGS [LZKS21, CZHS22, WGH⁺24] and neural networks [SBB24a] have been successfully used for SDE parameter estimation on real and synthetic data.

Third, our theory considers the infinite data setting, given the process’ true marginals $\{p_i\}_{i=0}^{N-1}$, and we have not studied asymptotic convergence rates. In particular, our identifiability result was established given continuously observed marginals, which corresponds to obtaining infinite samples from infinite marginals. Similarly, APPEX models the case where we obtain infinite samples from a finite set of marginals. We leave the asymptotics given the number of marginals N and the number of observations per marginal M for future work. Some theoretical considerations include the sample complexity of entropic optimal transport for trajectory inference, which requires asymptotically more samples per marginal as we decrease the entropic regularization (decreasing time granularity in the SDE setting) [GCB⁺19][Thm. 3], and the fact that the MLE of the AR(1) process from multiple trajectories is slightly biased [Led09]. We note that APPEX could

be combined with previous methods that relax the marginal constraints (see [LZKS21]). This could improve estimates in low data settings, particularly in the biological setting where taking measurements destroys samples.

Finally, even in the asymptotic setting, the nonconvex nature of APPEX’s alternating projection optimization problem makes the prospect of proving convergence difficult. Although our experiments indicate that APPEX’s estimates approach the true solution, regardless of the initial guesses for the drift A and observational diffusion H , we have not yet proved convergence due to the non-convexity of the optimization space. A formal proof of convergence and consistency would further strengthen its theoretical foundation.

Code Availability

The Python code for reproducing the experimental results and figures is available at <https://github.com/guanton/APPEX>. Analogous code in R is available at <https://github.com/HydroML/X0isAllYouNeed>.

Acknowledgements

The authors would like to thank United Therapeutics for supporting this research. GS and AW also acknowledge the support of the Burroughs Wellcome Fund.

References

- [AG92] E Eric Adams and Lynn W Gelhar. Field study of dispersion in a heterogeneous aquifer: 2. spatial moments analysis. *Water Resources Research*, 28(12):3293–3307, 1992.
- [Aka98] Hirotogu Akaike. Information theory and an extension of the maximum likelihood principle. In *Selected papers of Hirotogu Akaike*, pages 199–213. Springer, 1998.
- [Ari42] Aristotle. *Generation of Animals*, volume 366 of *Loeb Classical Library*. Harvard University Press, Cambridge, MA, 1942.
- [ATW⁺24] Lazar Atanackovic, Alexander Tong, Bo Wang, Leo J Lee, Yoshua Bengio, and Jason S Hartford. Dyngfin: Towards bayesian inference of gene regulatory networks with gflownets. *Advances in Neural Information Processing Systems*, 36, 2024.
- [AVI⁺20] Atte Aalto, Lauri Viitasaari, Pauliina Ilmonen, Laurent Mombaerts, and Jorge Gonçalves. Gene regulatory network inference from sparsely sampled noisy data. *Nature communications*, 11(1):3493, 2020.
- [BCDMN19] Jean-David Benamou, Guillaume Carlier, Simone Di Marino, and Luca Nenna. An entropy minimization approach to second-order variational mean-field games. *Mathematical Models and Methods in Applied Sciences*, 29(08):1553–1583, 2019.
- [BHCK23] Charlotte Bunne, Ya-Ping Hsieh, Marco Cuturi, and Andreas Krause. The schrödinger bridge between gaussian measures has a closed form. In *International Conference on Artificial Intelligence and Statistics*, pages 5802–5833. PMLR, 2023.
- [BHR93] Keith J Beven, D Ed Henderson, and Alison D Reeves. Dispersion parameters for undisturbed partially saturated soil. *Journal of hydrology*, 143(1-2):19–43, 1993.
- [Bis07] Jaya PN Bishwal. *Parameter estimation in stochastic differential equations*. Springer, 2007.
- [BLL⁺20] Philippe Brouillard, Sébastien Lachapelle, Alexandre Lacoste, Simon Lacoste-Julien, and Alexandre Drouin. Differentiable causal discovery from interventional data. *Advances in Neural Information Processing Systems*, 33:21865–21877, 2020.
- [BM24] Philip Boeken and Joris M Mooij. Dynamic structural causal models. *arXiv preprint arXiv:2406.01161*, 2024.

- [BPRF06] Alexandros Beskos, Omiros Papaspiliopoulos, Gareth O Roberts, and Paul Fearnhead. Exact and computationally efficient likelihood-based estimation for discretely observed diffusion processes (with discussion). *Journal of the Royal Statistical Society Series B: Statistical Methodology*, 68(3):333–382, 2006.
- [BYB⁺92] J Mark Boggs, Steven C Young, Lisa M Beard, Lynn W Gelhar, Kenneth R Rehfeldt, and E Eric Adams. Field study of dispersion in a heterogeneous aquifer: 1. overview and site description. *Water Resources Research*, 28(12):3281–3291, 1992.
- [Cam14] L Campbell. Reduction theorems for the strong real jacobian conjecture. In *Annales Polonici Mathematici*, volume 110, pages 1–11. Institute of Mathematics Polish Academy of Sciences, 2014.
- [CBL⁺19] Aaron G Cahill, Roger Beckie, Bethany Ladd, Elyse Sandl, Maximillian Goetz, Jessie Chao, Julia Soares, Cara Manning, Chitra Chopra, Niko Finke, et al. Advancing knowledge of gas migration and fugitive gas from energy wells in northeast british columbia, canada. *Greenhouse Gases: Science and Technology*, 9(2):134–151, 2019.
- [CCMV99] DW Chen, RF Carsel, L Moeti, and B Vona. Assessment and prediction of contaminant transport and migration at a florida superfund site. *Environmental monitoring and assessment*, 57:291–299, 1999.
- [CHLS23] Peter Craigmile, Radu Herbei, Ge Liu, and Grant Schneider. Statistical inference for stochastic differential equations. *Wiley Interdisciplinary Reviews: Computational Statistics*, 15(2):e1585, 2023.
- [CHS22] Megan A Coomer, Lucy Ham, and Michael PH Stumpf. Noise distorts the epigenetic landscape and shapes cell-fate decisions. *Cell Systems*, 13(1):83–102, 2022.
- [CML09] Paramita Chakraborty, Mark M Meerschaert, and Chae Young Lim. Parameter estimation for fractional transport: A particle-tracking approach. *Water resources research*, 45(10), 2009.
- [CZHS22] Lénaïc Chizat, Stephen Zhang, Matthieu Heitz, and Geoffrey Schiebinger. Trajectory inference via mean-field langevin in path space. *Advances in Neural Information Processing Systems*, 35:16731–16742, 2022.
- [DAD05] Frédéric Delay, Philippe Ackerer, and Charles Danquigny. Simulating solute transport in porous or fractured formations using random walk particle tracking: A review. *Vadose Zone Journal*, 4(2):360–379, 2005.
- [Did08] Vanessa Didelez. Graphical models for marked point processes based on local independence. *Journal of the Royal Statistical Society Series B: Statistical Methodology*, 70(1):245–264, 2008.
- [Doo42] Joseph L Doob. The brownian movement and stochastic equations. *Annals of Mathematics*, 43(2):351–369, 1942.
- [Elf06] Amro MM Elfeki. Prediction of contaminant plumes (shapes, spatial moments and macrodispersion) in aquifers with insufficient geological information. *Journal of Hydraulic Research*, 44(6):841–856, 2006.
- [FG20] Wei Fang and Michael B Giles. Adaptive euler–maruyama method for sdes with nonglobally lipschitz drift. *The Annals of Applied Probability*, 30(2):526–560, 2020.
- [FMR06] EO Frind, JW Molson, and DL Rudolph. Well vulnerability: a quantitative approach for source water protection. *Groundwater*, 44(5):732–742, 2006.
- [For24] Aden Farrow. Consistent diffusion matrix estimation from population time series. *arXiv preprint arXiv:2408.14408*, 2024.
- [FWR⁺18] Jeffrey A Farrell, Yiqun Wang, Samantha J Riesenfeld, Karthik Shekhar, Aviv Regev, and Alexander F Schier. Single-cell reconstruction of developmental trajectories during zebrafish embryogenesis. *Science*, 360(6392):eaar3131, 2018.

- [GCB⁺19] Aude Genevay, Lénaïc Chizat, Francis Bach, Marco Cuturi, and Gabriel Peyré. Sample complexity of sinkhorn divergences. In *The 22nd international conference on artificial intelligence and statistics*, pages 1574–1583. PMLR, 2019.
- [Gil00] Daniel T Gillespie. The chemical langevin equation. *The Journal of Chemical Physics*, 113(1):297–306, 2000.
- [GNB22] Promit Ghosal, Marcel Nutz, and Espen Bernton. Stability of entropic optimal transport and schrödinger bridges. *Journal of Functional Analysis*, 283(9):109622, 2022.
- [HC15] Miranda Holmes-Cerfon. Applied stochastic analysis, 2015.
- [HGJ16] Tatsunori Hashimoto, David Gifford, and Tommi Jaakkola. Learning population-level diffusions with generative rnns. In *International Conference on Machine Learning*, pages 2417–2426. PMLR, 2016.
- [HS14] Niels Hansen and Alexander Sokol. Causal interpretation of stochastic differential equations. *Electronic Journal of Probability*, 2014.
- [HSKP08] Patrik O Hoyer, Shohei Shimizu, Antti J Kerminen, and Markus Palviainen. Estimation of causal effects using linear non-gaussian causal models with hidden variables. *International Journal of Approximate Reasoning*, 49(2):362–378, 2008.
- [Hua24] Hanwen Huang. One-step data-driven generative model via schrödinger bridge. *arXiv preprint arXiv:2405.12453*, 2024.
- [HZL⁺23] Mónica Basilio Hazas, Francesca Ziliotto, Jonghyun Lee, Massimo Rolle, and Gabriele Chiogna. Evolution of plume geometry, dilution and reactive mixing in porous media under highly transient flow fields at the surface water-groundwater interface. *Journal of Contaminant Hydrology*, 258:104243, 2023.
- [Jan21] Hicham Janati. *Advances in Optimal transport and applications to neuroscience*. PhD thesis, Institut Polytechnique de Paris, 2021.
- [KOLL12] SC Kou, Benjamin P Olding, Martin Lysy, and Jun S Liu. A multiresolution method for parameter estimation of diffusion processes. *Journal of the American Statistical Association*, 107(500):1558–1574, 2012.
- [LBSV⁺19] Luca Locatelli, Philip J Binning, Xavier Sanchez-Vila, Gitte Lemming Søndergaard, Louise Rosenberg, and Poul L Bjerg. A simple contaminant fate and transport modelling tool for management and risk assessment of groundwater pollution from contaminated sites. *Journal of contaminant hydrology*, 221:35–49, 2019.
- [Led09] Johannes Ledolter. Estimation bias in the first-order autoregressive model and its impact on predictions and prediction intervals. *Communications in Statistics-Simulation and Computation*, 38(4):771–787, 2009.
- [LES03] Russell Lande, Steinar Engen, and Bernt-Erik Saether. *Stochastic population dynamics in ecology and conservation*. Oxford University Press, USA, 2003.
- [LJP⁺21] Lu Lu, Pengzhan Jin, Guofei Pang, Zhongqiang Zhang, and George Em Karniadakis. Learning nonlinear operators via deepnet based on the universal approximation theorem of operators. *Nature machine intelligence*, 3(3):218–229, 2021.
- [LKR02] Peter C Lichtner, Sharad Kelkar, and Bruce Robinson. New form of dispersion tensor for axisymmetric porous media with implementation in particle tracking. *Water Resources Research*, 38(8):21–1, 2002.
- [LKS24] Lars Lorch, Andreas Krause, and Bernhard Schölkopf. Causal modeling with stationary diffusions. In *International Conference on Artificial Intelligence and Statistics*, pages 1927–1935. PMLR, 2024.

- [LRW21] Yiheng Liu, Elina Robeva, and Huanqing Wang. Learning linear non-gaussian graphical models with multidirected edges. *Journal of Causal Inference*, 9(1):250–263, 2021.
- [LZKS21] Hugo Lavenant, Stephen Zhang, Young-Heon Kim, and Geoffrey Schiebinger. Towards a mathematical theory of trajectory inference. *arXiv preprint arXiv:2102.09204*, 2021.
- [MCF⁺24] Georg Manten, Cecilia Casolo, Emilio Ferrucci, Søren Wengel Mogensen, Cristopher Salvi, and Niki Kilbertus. Signature kernel conditional independence tests in causal discovery for stochastic processes. *arXiv preprint arXiv:2402.18477*, 2024.
- [MFRC86] DM Mackay, DL Freyberg, PV Roberts, and JA Cherry. A natural gradient experiment on solute transport in a sand aquifer: 1. approach and overview of plume movement. *Water Resources Research*, 22(13):2017–2029, 1986.
- [MH20] Søren Wengel Mogensen and Niels Richard Hansen. Markov equivalence of marginalized local independence graphs. *The Annals of Statistics*, 48(1):539–559, 2020.
- [MH22] Søren Wengel Mogensen and Niels Richard Hansen. Graphical modeling of stochastic processes driven by correlated noise. *Bernoulli*, 28(4):3023–3050, 2022.
- [MHB16] Stephan Mandt, Matthew Hoffman, and David Blei. A variational analysis of stochastic gradient algorithms. In *International conference on machine learning*, pages 354–363. PMLR, 2016.
- [MMP15] Kevin McGoff, Sayan Mukherjee, and Natesh Pillai. Statistical inference for dynamical systems: A review. *Statist. Surv.*, 2015.
- [MT07] Chuanjian Man and Christina W Tsai. Stochastic partial differential equation-based model for suspended sediment transport in surface water flows. *Journal of engineering mechanics*, 133(4):422–430, 2007.
- [NM24] Ahmed Nafidi and İlyasse Makroz. A comparison of methods for estimating parameters of the stochastic lomax process: through simulation study. *Hacettepe Journal of Mathematics and Statistics*, 53(2):495–505, 2024.
- [NMY00] Jan Nygaard Nielsen, Henrik Madsen, and Peter C Young. Parameter estimation in stochastic differential equations: an overview. *Annual Reviews in Control*, 24:83–94, 2000.
- [NR20] Richard Nickl and Kolyan Ray. Nonparametric statistical inference for drift vector fields of multi-dimensional diffusions. *The Annals of Statistics*, 48(3):1383–1408, 2020.
- [Nut21] Marcel Nutz. Introduction to entropic optimal transport. *Lecture notes, Columbia University*, 2021.
- [O⁺82] William Ogle et al. *Aristotle: on the parts of animals*. Kegan Paul, French & Company, 1882.
- [O⁺02] Dennis R O’Connor et al. Part two: Report of the walkerton inquiry: A strategy for safe drinking water. Technical report, Ministry of the Attorney General, 2002.
- [Oks13] Bernt Oksendal. *Stochastic differential equations: an introduction with applications*. Springer Science & Business Media, 2013.
- [OT10] Jungsun Oh and Christina W Tsai. A stochastic jump diffusion particle-tracking model (sjd-ptm) for sediment transport in open channel flows. *Water Resources Research*, 46(10), 2010.
- [Özd16] Mustafa Özdemir. An alternative approach to elliptical motion. *Advances in Applied Clifford Algebras*, 26:279–304, 2016.
- [Pau97] Anthony J Paulson. The transport and fate of fe, mn, cu, zn, cd, pb and so4 in a groundwater plume and in downstream surface waters in the coeur d’alene mining district, idaho, usa. *Applied Geochemistry*, 12(4):447–464, 1997.
- [Pav14] Grigorios A Pavliotis. Stochastic processes and applications. *Texts in Applied Mathematics*, 60, 2014.

- [PC⁺19] Gabriel Peyré, Marco Cuturi, et al. Computational optimal transport: With applications to data science. *Foundations and Trends® in Machine Learning*, 11(5-6):355–607, 2019.
- [PHR19] Rich Pawlowicz, Charles Hannah, and Andy Rosenberger. Lagrangian observations of estuarine residence times, dispersion, and trapping in the salish sea. *Estuarine, Coastal and Shelf Science*, 225:106246, 2019.
- [PMA03] S Peiris, R Mellor, and P Ainkaran. Maximum likelihood estimation for short time series with replicated observations: A simulation study. *InterStat*, 9:1–16, 2003.
- [PP⁺08] Kaare Brandt Petersen, Michael Syskind Pedersen, et al. The matrix cookbook. *Technical University of Denmark*, 7(15):510, 2008.
- [RCM⁺24] Martin Rohbeck, Brian Clarke, Katharina Mikulik, Alexandra Pettet, Oliver Stegle, and Kai Ueltzhöffer. Bicycle: Intervention-based causal discovery with cycles. In *Causal Learning and Reasoning*, pages 209–242. PMLR, 2024.
- [RSW21] Alexander Reisch, Christof Seiler, and Sebastian Weichwald. Beware of the simulated dag! causal discovery benchmarks may be easy to game. *Advances in Neural Information Processing Systems*, 34:27772–27784, 2021.
- [Run21] Jakob Runge. Necessary and sufficient graphical conditions for optimal adjustment sets in causal graphical models with hidden variables. *Advances in Neural Information Processing Systems*, 34:15762–15773, 2021.
- [SBB24a] Yunyi Shen, Renato Berlinghieri, and Tamara Broderick. Learning a vector field from snapshots of unidentified particles rather than particle trajectories. In *ICLR 2024 Workshop on AI4DifferentialEquations In Science*, 2024.
- [SBB24b] Yunyi Shen, Renato Berlinghieri, and Tamara Broderick. Multi-marginal schrödinger bridges with iterative reference. *arXiv preprint arXiv:2408.06277*, 2024.
- [SFGGH07] Peter Salamon, Daniel Fernández-García, and JJ Gómez-Hernández. Modeling tracer transport at the made site: The importance of heterogeneity. *Water Resources Research*, 43(8), 2007.
- [SHH⁺06] Shohei Shimizu, Patrik O Hoyer, Aapo Hyvärinen, Antti Kerminen, and Michael Jordan. A linear non-gaussian acyclic model for causal discovery. *Journal of Machine Learning Research*, 7(10), 2006.
- [SS19] Simo Särkkä and Arno Solin. *Applied stochastic differential equations*, volume 10. Cambridge University Press, 2019.
- [SST⁺19] Geoffrey Schiebinger, Jian Shu, Marcin Tabaka, Brian Cleary, Vidya Subramanian, Aryeh Solomon, Joshua Gould, Siyan Liu, Stacie Lin, Peter Berube, et al. Optimal-transport analysis of single-cell gene expression identifies developmental trajectories in reprogramming. *Cell*, 176(4):928–943, 2019.
- [Str08] Daniel W Stroock. *Partial differential equations for probabilists [sic]*. Cambridge University Press, 2008.
- [STRZ⁺16] Manu Setty, Michelle D Tadmor, Shlomit Reich-Zeliger, Omer Angel, Tomer Meir Salame, Pooja Kathail, Kristy Choi, Sean Bendall, Nir Friedman, and Dana Pe’er. Wishbone identifies bifurcating developmental trajectories from single-cell data. *Nature biotechnology*, 34(6):637–645, 2016.
- [TB13] Shahab Torkamani and Eric A Butcher. Stochastic parameter estimation in nonlinear time-delayed vibratory systems with distributed delay. *Journal of Sound and Vibration*, 332(14):3404–3418, 2013.
- [TCG⁺14] Cole Trapnell, Davide Cacchiarelli, Jonna Grimsby, Prapti Pokharel, Shuqiang Li, Michael Morse, Niall J Lennon, Kenneth J Livak, Tarjei S Mikkelsen, and John L Rinn. The dynamics and regulators of cell fate decisions are revealed by pseudotemporal ordering of single cells. *Nature biotechnology*, 32(4):381–386, 2014.

- [TLBB⁺23] Alejandro Tejada-Lapuerta, Paul Bertin, Stefan Bauer, Hananeh Aliee, Yoshua Bengio, and Fabian J Theis. Causal machine learning for single-cell genomics. *arXiv preprint arXiv:2310.14935*, 2023.
- [VTLL21] Francisco Vargas, Pierre Thodoroff, Austen Lamacraft, and Neil Lawrence. Solving schrödinger bridges via maximum likelihood. *Entropy*, 23(9):1134, 2021.
- [Wad35] CH Waddington. How animal develop, 1935.
- [Wad57] CH Waddington. *The strategy of the genes: a discussion of some aspects of theoretical biology*. London: Allen and Unwin, 1957.
- [WGH⁺24] Yuanyuan Wang, Xi Geng, Wei Huang, Biwei Huang, and Mingming Gong. Generator identification for linear sdes with additive and multiplicative noise. *Advances in Neural Information Processing Systems*, 36, 2024.
- [Whi82] Halbert White. Maximum likelihood estimation of misspecified models. *Econometrica: Journal of the econometric society*, pages 1–25, 1982.
- [WT74] Richard E Williamson and Hale F Trotter. Multivariable mathematics: linear algebra, differential equations, calculus. (*No Title*), 1974.
- [WTW⁺23] Lingfei Wang, Nikolaos Trasanidis, Ting Wu, Guanlan Dong, Michael Hu, Daniel E Bauer, and Luca Pinello. Dictys: dynamic gene regulatory network dissects developmental continuum with single-cell multiomics. *Nature Methods*, 20(9):1368–1378, 2023.
- [WWT⁺18] Caleb Weinreb, Samuel Wolock, Betsabeh K Tusi, Merav Socolovsky, and Allon M Klein. Fundamental limits on dynamic inference from single-cell snapshots. *Proceedings of the National Academy of Sciences*, 115(10):E2467–E2476, 2018.
- [YWI⁺23] Toshiaki Yachimura, Hanbo Wang, Yusuke Imoto, Momoko Yoshida, Sohei Tasaki, Yoji Kojima, Yukihiro Yabuta, Mitinori Saitou, and Yasuaki Hiraoka. scegot: Single-cell trajectory inference framework based on entropic gaussian mixture optimal transport. *bioRxiv*, pages 2023–09, 2023.
- [Zha24] Stephen Y Zhang. Joint trajectory and network inference via reference fitting. *arXiv preprint arXiv:2409.06879*, 2024.
- [ZLSS24] Wenjun Zhao, Erica Larschan, Bjorn Sandstede, and Ritambhara Singh. Optimal transport reveals dynamic gene regulatory networks via gene velocity estimation. *bioRxiv*, pages 2024–09, 2024.

8 Appendix

8.1 SDEs and causality

Let V be a set of d endogenous variables $\{X^{(1)}, X^{(d)}\}$ and W be a set of exogenous variables $\{X^{(d+1)}, X^{(d+r)}\}$, which are excluded from the principal model, but may influence the endogenous variables. Suppose that all variables evolve according to a general SDE, which can be written in “integrand-integrator” form

$$dX_t = a(t, X_t) dh(t, X_t). \quad (39)$$

By integrating and considering each variable $X_t^{(j)}$ in the endogenous set $j \in V$, [BM24] showed that we can define a dynamic structural causal model (DSCM) [Definition 1]:

$$X_t^{(j)} = X_0^{(j)} + \int_0^t a_j(s, X_s^{\alpha(j)}) dh_j(s, X_s^{\beta(j)}), \quad (40)$$

where $\alpha(j), \beta(j) \subset V \cup W$ represent the variables that are used as arguments for $a_j(t, X_t)$ and $h_j(t, X_t)$ respectively. In particular, (40) defines a causal graph \mathcal{G} with vertices $V \cup W$, and edges $E = \{i \rightarrow j : j \in V, i \in \alpha(j) \cup \beta(j)\}$ [BM24][Definition 2]. In other words, we only consider edges that point towards variables in the endogenous set, and we include the edge $i \rightarrow j$ if $X^{(i)}$ influences the evolution of endogenous variable $X^{(j)}$ through the integrand $a_j(t, X_t)$ or integrator $h_j(t, X_t)$. Additionally, in [BM24], self-loops $j \rightarrow j$ are excluded to have a simple SCM, but we do not follow this convention in this paper. Under this more general framework, we see that latent confounders can affect endogenous variables via the integrand or integrator, which can be decoupled as drift and diffusion. For instance, any SDE driven by Brownian motion

$$dX_t = b(t, X_t) dt + \sigma(t, X_t) dW_t, \quad (41)$$

can be rewritten in the form (39) by setting $a(t, X_t) = [b(t, X_t) \quad \sigma(t, X_t)]$ and $h(t, X_t) = [t \quad W_t]^T$. Given that $X_t \in \mathbb{R}^d$, $W_t \in \mathbb{R}^m$, we have corresponding dimensions $b(X_t) \in \mathbb{R}^d$, $\sigma(X_t) \in \mathbb{R}^{d \times m}$, $Z_t \in \mathbb{R}^{m+1}$, and $\alpha(X_t) \in \mathbb{R}^{d \times (m+1)}$. The DSCM can therefore also be written as

$$X_t^{(j)} = X_0^{(j)} + \int_0^t b_j(s, X_s^{\alpha(j)}) ds + \int_0^t \sigma(s, X_s^{\beta(j)}) dW_s. \quad (42)$$

DSCMs observe graphical Markov properties under local independence [Did08, MH20, MH22] under the assumption of independent driving noise, also known as independent integrators [BM24][Theorem 4]. This is formally defined as $\beta(j) \subset W$ and $\beta(i) \cap \beta(j) = \emptyset$ for all $i, j \in V$.

Example 8.1 (Non-identifiability of higher order multidirected edges). *Consider two matrices G_1, G_2 , which share the same observational diffusion H :*

$$G_1 = \begin{bmatrix} 0 & 1 & 1 \\ 1 & 0 & 1 \\ 1 & 1 & 0 \end{bmatrix}, \quad G_2 = \begin{bmatrix} \frac{4}{3} & \frac{1}{3} & \frac{1}{3} \\ \frac{1}{3} & \frac{4}{3} & \frac{1}{3} \\ \frac{1}{3} & \frac{1}{3} & \frac{4}{3} \end{bmatrix}, \quad H = G_1 G_1^T = G_2 G_2^T = \begin{bmatrix} 2 & 1 & 1 \\ 1 & 2 & 1 \\ 1 & 1 & 2 \end{bmatrix}$$

Given G_1 as the additive noise of an SDE, each pair of variables shares a noise source, since each row shares a nonzero column entry with another row. However, there is no common noise source that is shared among all 3 variables, since each column contains a 0. Hence, the causal interpretation under G_1 consists in three bidirected edges $1 \leftrightarrow 2$, $1 \leftrightarrow 3$, $2 \leftrightarrow 3$. In contrast, the causal interpretation under G_2 consists in a single multidirected edge $(1, 2, 3)$, since all components share noise sources.

Since G_1 and G_2 admit different causal graphs, despite having the same observational diffusion H , this shows that H provides information about the existence of unobserved confounders between pairs of variables, but cannot provide further causal structure about the confounder with respect to the other endogenous variables $[d] \setminus \{i, j\}$.

We note that if the noise is not additive, then this further complicates the causal interpretation. In this case, the driving noise $\sigma(X_t)$ may be a function of the endogenous variables, i.e. $\beta(j) \cap V \neq \emptyset$. Thus, unlike the additive noise setting in Theorem 4.5, simple edges $i \rightarrow j$ may be informed by the driving noise, via $\beta(j)$, rather than just the drift, via $\alpha(j)$. However, since only $\sigma(X_t)\sigma(X_t)^T$ is observable rather than $\sigma(X_t)$ itself, observational data under such a model would lend itself to multiple interpretations of the causal graph. The idea is similar to Example 8.1, where we saw one interpretation feature three bidirected edges and another feature a multi-edge, but under non-additive noise, the ambiguity extends to simple edges $i \rightarrow j$. This is illustrated in Example 5.5 in [HS14].

8.2 Weak formulation of Fokker-Planck

We may define the linear operator \mathcal{L}

$$(\mathcal{L}f)(x) = b(x) \cdot f(x) + \frac{1}{2} \nabla \cdot (H \nabla f(x)),$$

\mathcal{L} is the generator of the additive noise SDE (1) [HC15]. Its adjoint operator is given by

$$(\mathcal{L}^*g)(x) = -\nabla \cdot (b(x, t)g(x)) + \nabla \cdot (H \nabla g(x)).$$

and satisfies

$$\int_{\mathbb{R}^d} \mathcal{L}f(x)g(x) dx = \langle \mathcal{L}f, g \rangle = \langle f, \mathcal{L}^*g \rangle = \int_{\mathbb{R}^d} f(x)\mathcal{L}^*g(x) dx,$$

for all smooth and compactly supported test functions $f, g \in C_c^\infty(\mathbb{R}^d)$.

Then, the Fokker-Planck equation can be formulated in the weak sense as follows. For each $t \geq 0$ let p_t be a probability measure on \mathbb{R}^d and assume that $t \mapsto p_t$ is narrowly continuous. Then we say p_t solves the Fokker-Planck equation in the weak sense provided that

$$\frac{d}{dt} \int \varphi(x) dp_t(x) = \int \mathcal{L}\varphi(x) dp_t(x) \quad \forall \varphi \in C_c^2(\mathbb{R}^d).$$

This weak formulation accommodates the case where b is not differentiable and p_t is not necessarily absolutely continuous with respect to the Lebesgue measure. For p_t with sufficiently regular Lebesgue density $p(x, t)$ this weak solution concept is equivalent to the classical sense of the Fokker-Planck equation, i.e.

$$\partial_t p(x, t) = \mathcal{L}^*p(x, t).$$

For the measure-theoretic weak formulation of the Fokker-Planck equation, we quote the following existence and uniqueness results from [Str08]. Under our standing assumptions on the drift and diffusion coefficients (namely: the drift is linear, and the diffusion is constant but possibly degenerate), by [Str08] Theorem 1.1.9 weak solutions to the Fokker-Planck equation exist whenever the initial condition ρ_0 has finite second moments; and moreover, by Theorem 2.2.9 in [Str08], the solution is unique provided that all moments of ρ_0 are finite.

8.3 Generalized rotations and additional proofs

Definition 8.2. A rotation in \mathbb{R}^d is defined via the matrix exponential map e^{At} where $A \in \mathbb{R}^{d \times d}$ is skew-symmetric, i.e. $A + A^T = 0$.

Example 8.3. The unit sphere in \mathbb{R}^d

$$S^{d-1} = \{x \in \mathbb{R}^d : x^T x = 1\}$$

is rotationally invariant, i.e. $\forall t \geq 0, e^{At}S^{d-1} = S^{d-1}$ for a skew-symmetric matrix A , i.e. $A + A^T = 0$.

Proof. For any $x \in S^{d-1}$, we have $y = e^{At}x \in S^{d-1}$, since

$$y^T y = (e^{At}x)^T e^{At}x = x^T e^{A^T t} e^{At}x = x^T e^{(A+A^T)t}x = x^T x = 1.$$

Similarly, the inverse map $y = e^{-At}x \in S^{d-1}$. □

Example 8.4. Let $\Sigma \succ 0$ and $r > 0$. An ellipsoid defined by the quadratic form

$$E_\Sigma = \{x \in \mathbb{R}^d : x^T \Sigma^{-1} x = r\}$$

is Σ -rotationally invariant, i.e. $\forall t \geq 0, e^{At}E_\Sigma = E_\Sigma$ if $A\Sigma + \Sigma A^T = 0$.

Proof. For any $x \in E_\Sigma$, we have $y = e^{At}x \in E_\Sigma$, since

$$y^T \Sigma y = (e^{At}x)^T \Sigma e^{At}x = x^T (e^{A^T t} \Sigma e^{At})x = x^T \Sigma x = 1.$$

Lemma 8.7 was applied in the penultimate step. Similarly, the inverse map $y = e^{-At}x \in E_\Sigma$. □

Lemma 8.5. Let X be a r.v. with covariance Σ and suppose that $e^{At}X \sim X$. Then, $A\Sigma + \Sigma A^T = 0$.

Proof. Let $C(t) = \text{Cov}(e^{At}X)$. $e^{At}X \sim X$ implies that for all $t \geq 0$, $C(t) = \text{Cov}(X) = \Sigma$. Hence,

$$\begin{aligned} C(t) &= e^{At}\Sigma e^{A^T t} = \Sigma \\ C'(t) &= Ae^{At}\Sigma e^{A^T t} + e^{At}\Sigma A^T e^{A^T t} = 0 \\ C'(0) &= A\Sigma + \Sigma A^T = 0. \end{aligned}$$

□

Lemma 8.6. Let $\text{Cov}(X) = \Sigma \succ 0$ and suppose that X is auto-rotationally invariant. Then X admits a density, and the level sets of its probability density function are Σ -rotationally invariant ellipsoids:

$$\text{Let } E_{\Sigma}^{(k)} = \{x \in \mathbb{R}^d : x^T \Sigma^{-1} x = k\}, \text{ then } \forall x, y \in E_{\Sigma}^{(k)}, p(x) = p(y) \quad (43)$$

Proof. If X is auto-rotationally invariant, then there is a Σ -generalized rotation $e^{At}X \sim X$ with $A \neq 0$. Equivalently, $p(x) = p(e^{At}x)$ for all $x \in \mathbb{R}^d$. Since $e^{At}E_{\Sigma}^{(k)} = E_{\Sigma}^{(k)}$, the probability distribution of X must be constant within each ellipsoid $E_{\Sigma}^{(k)}$. Since $\Sigma \succ 0$, then each set $E_{\Sigma}^{(k)}$ is non-degenerate in \mathbb{R}^d , thus inducing a probability density function on X . □

Lemma 8.7. Given $A\Sigma + \Sigma A^T = 0$, it follows that

$$(e^{At})^T \Sigma e^{At} = \Sigma.$$

Proof. Let $M(t) = (e^{At})^T \Sigma e^{At}$. Then,

$$\begin{aligned} \frac{d}{dt}M(t) &= (Ae^{At})^T \Sigma e^{At} + (e^{At})^T \Sigma (Ae^{At}) \\ &= e^{A^T t} (A^T \Sigma + \Sigma A) e^{At} = 0, \end{aligned}$$

where we used $A\Sigma + \Sigma A^T = 0$ in the last step. Hence, $M(t) = (e^{At})^T \Sigma e^{At} = M(0) = \Sigma$ □

Lemma 8.8. Let X be a d dimensional r.v. such that $\dim(\text{span}(X)) < d$ with probability 1. Then,

$$e^{At}X \sim X$$

admits a non-trivial solution $A \neq 0$.

Proof. We expand

$$e^{At}X = X + \left(\sum_{n=1}^{\infty} \frac{t^n}{n!} A^n \right) X$$

Hence, a sufficient condition for the claim is that X is in the nullspace of A with probability 1. Since $\dim(\text{span}(X)) < d$ a.s., then by the rank-nullity theorem, there exists A such that $AX = 0$ a.s. □

Lemma 8.9. Let $\Sigma \succeq 0$ be a symmetric positive semidefinite matrix and suppose that A is skew-symmetric with respect to Σ , i.e.

$$A\Sigma + \Sigma A^T = 0,$$

then without loss of generality, we may define A with $\text{Tr}(A) = 0$.

Proof.

$$\text{Tr}(A\Sigma + \Sigma A^T) = \text{Tr}(0) = 0.$$

Using the linearity of the trace and the cyclic property $\text{Tr}(XY) = \text{Tr}(YX)$:

$$\begin{aligned}\text{Tr}(A\Sigma + \Sigma A^T) &= \text{Tr}(A\Sigma) + \text{Tr}(A^T\Sigma) \\ &= \text{Tr}(A\Sigma) + \text{Tr}(\Sigma A) \\ &= 2\text{Tr}(A\Sigma).\end{aligned}$$

Therefore,

$$2\text{Tr}(A\Sigma) = 0 \quad \Rightarrow \quad \text{Tr}(A\Sigma) = 0.$$

If $\Sigma \succ 0$, then we immediately conclude $\text{Tr}(A) = 0$. Otherwise, we may pick A such that $\Sigma_{i,i} = 0 \Rightarrow A_{i,i} = 0$ to ensure that $\text{Tr}(A) = 0$. \square

Corollary 8.10. *If A is skew-symmetric with respect to Σ , and $\Sigma \succ 0$, then Ax is a divergence-free vector field:*

$$\nabla \cdot Ax = 0$$

Proof. We know that

$$\begin{aligned}\nabla \cdot Ax &= \sum_{i=1}^d \frac{\partial}{\partial x_i} (A_i x) \\ &= \sum_{i=1}^d \frac{\partial}{\partial x_i} \sum_{j=1}^d (A_{i,j} x_j) \\ &= \sum_{i=1}^d A_{i,i} = \text{Tr}(A),\end{aligned}$$

which is 0 by Lemma 8.9. \square

Proposition 8.11. *Let $X_0 \sim p_0$ be a discrete random variable. Then X_0 is not auto-rotationally invariant if and only if the support of p_0 spans \mathbb{R}^d .*

Proof. Lemma 8.8 provides the only if direction.

Now, let $\text{span}(X_0) = \mathbb{R}^d$ a.s. Since e^{At} represents a continuous transformation, and X_0 is supported on a discrete set of points, which cannot all be mapped to 0 by A , it follows that the support would shift for each $t > 0$. We conclude that $e^{At}X_0 \not\sim X_0$. \square

Lemma 8.12. *As in Theorem 4.3, let X_0 have covariance $\Sigma = GG^T$ be auto-rotationally invariant, such that $e^{As}X_0 \sim X_0 \forall s \geq 0$, and consider the SDEs*

$$dX_t = \gamma G dW_t \tag{44}$$

$$dX_t = AX_t dt + \gamma G dW_t. \tag{45}$$

Then, X_t will also be auto-rotationally invariant, such that $e^{As}X_t \sim X_t \forall s \geq 0$.

Proof. Since both SDEs are linear additive noise, they admit closed form solutions. For the first SDE (44), we have

$$X_t = X_0 + \gamma \int_0^t G dW_s.$$

Moreover, because the SDE parameters A, G obey $GG^T = \Sigma$ and $A\Sigma + \Sigma A^T = 0$ by construction, then by the Σ -rotational invariance of $\mathcal{N}(0, \Sigma)$, we have

$$GdW_s \sim \mathcal{N}(0, \Sigma ds) \sim e^{A(t-s)} GdW_s.$$

We may therefore write the solution of the first SDE (44) as

$$X_t = X_0 + \gamma \int_0^t e^{A(t-s)} GdW_s.$$

Hence, $X_t \sim X_0 + M_t$, where $M_t = \gamma \int_0^t e^{A(t-s)} G dW_s \sim \mathcal{N}(0, \gamma^2 \Sigma)$. Since X_0 and M_t are each auto-rotationally invariant with respect to the map e^{As} , while being independent due to the independent increments of Brownian motion, it follows that $X_t \sim X_0 + M_t$ is also auto-rotationally invariant with respect to the map e^{As} . We immediately recognize the same conclusion for the second SDE (45), since its closed solution is the same in distribution to the first SDE:

$$X_t = e^{At} X_0 + \gamma \int_0^t e^{A(t-s)} G dW_s \sim X_0 + \gamma \int_0^t e^{A(t-s)} G dW_s.$$

□

Proof of Theorem 4.3 for general probability measures. The general argument for Theorem 4.3 applies even in the case where $p(x, t)$ is a general probability measure, since we can instead work with the weak formulation of the Fokker-Planck equation.

For the first direction, it suffices to show that for all $\varphi \in C_c^2(\mathbb{R}^d)$, we have that

$$\int (\nabla \varphi(x) \cdot Ax) dp_t(x) = 0$$

since this corresponds to the weak formulation of the divergence term $\nabla \cdot (p_t(x)Ax)$. Integrating by parts, we see that

$$\int (\nabla \varphi(x) \cdot Ax) dp_t(x) = - \int \varphi(x) \nabla \cdot (Ax) dp_t(x).$$

We have already established that $\nabla \cdot (Ax) = 0$, hence $\varphi(x) \nabla \cdot (Ax) = 0$ also. The claim follows.

For the second direction, we just need to check that p_0 is also the stationary distribution of the residual SDE when the temporal marginals p_t are general measures. To do so, we compute the weak formulation of the Fokker-Planck equation (16). For each t , let p_t denote the probability measure which is the distribution of X_t . For any test function $\varphi \in C_c^2(\mathbb{R}^d)$,

$$\frac{d}{dt} \int \varphi(x) dp_t(x) = \int L^* \varphi(x) dp_t(x) = \int L_1^* \varphi(x) dp_t(x)$$

which implies that for all t

$$0 = \int (L - L_1)^* \varphi(x) dp_t(x). \quad (46)$$

Now we take $L - L_1$ to be the differential operator for the residual SDE. From the uniqueness theory for the weak solutions of the Kolmogorov forward equation (see [Str08] Thm. 2.2.9) it follows that as long as $p(x, 0)$ has finite moments of all orders, then there is exactly one weakly continuous solution $\mu_t : [0, T] \rightarrow \mathcal{P}(\mathbb{R}^d)$ beginning at p_0 satisfying, for all $\varphi \in C_c^2(\mathbb{R}^d)$

$$\frac{d}{dt} \int \varphi(x) d\mu_t(x) = \int (L - L_1)^* \varphi(x) d\mu_t(x).$$

This implies that for the initial condition p_0 , we have in particular that $0 = \int (L - L_1)^* \varphi(x) dp_0(x)$, which implies that $\frac{d}{dt} \int \varphi(x) d\mu_t(x)|_{t=0} = 0$. Hence, $\mu_t = p_t$, which is the stationary solution to (46) as desired. □

The linear additive noise SDE can be generalized to accommodate a constant drift μ :

$$dX_t = (AX_t + \mu) dt + G dW_t, X_0 \sim p_0 \quad (47)$$

Corollary 8.13. *Let the initial distribution p_0 have finite support on $d + 1$ vectors $\{x_i : x_i \in \mathbb{R}^d\}_{i=1}^{d+1}$ spanning \mathbb{R}^d such that each pair of vectors are linearly independent. If X_t evolves according to an arbitrary d -dimensional linear additive noise SDE with an additional constant drift μ : (47), then μ, A , and GG^T of the SDE are uniquely identified from temporal marginals.*

Proof. Following the same argument as Theorem 4.3, we obtain a deterministic residual SDE with respect to $X_0 \sim p(x, 0)$:

$$\frac{dX_t}{dt} = \bar{A}X_t + \bar{\mu} = 0.$$

This implies that $\bar{A}x_i = -\bar{\mu}$ for each of the $d + 1$ vectors x_i in the support of p_0 . Equivalently, since each pair of vectors is linearly independent, we can write

$$\bar{A}(x_i - x_j) = 0,$$

such that the differences $x_i - x_j$ span \mathbb{R}^d . The rank-nullity theorem implies that $\bar{A} = 0$ and hence $\bar{\mu} = 0$. \square

Proposition 8.14. *The strong solution to the linear additive noise SDE (2) is*

$$X_t = e^{At}X_0 + \int_0^t e^{A(t-s)}GdW_s \quad (48)$$

Proof. This result has been proven in [SS19][Sec 4.3] via the integrating factor e^{-At} . \square

Corollary 8.15. *The transition kernel of the linear additive noise SDE (2) is the Gaussian*

$$X_{t+\Delta t}|X_t = x \sim \mathcal{N}(e^{A\Delta t}x, \int_0^{\Delta t} e^{A(\Delta t-s)}He^{A^T(\Delta t-s)}ds) \quad (49)$$

8.4 Revisiting non-identifiability examples

The proof of Theorem (4.3) provides a nice characterization of non-identifiability. A pair of SDEs are non-identifiable with respect to one another given $p(x, 0)$ only if $p(x, 0)$ is a stationary distribution with respect to their residual SDE.

Pair 1: Starting at stationary

In this example, the residual SDE is given by

$$dX_t = -9X_t dt + \sqrt{9}dW_t,$$

for which $\mathcal{N}(0, \frac{1}{2})$ is a stationary distribution, which is consistent with non-identifiability from $p_0 \sim \mathcal{N}(0, \frac{1}{2})$. However, it is obvious that a discrete probability distribution cannot be stationary with respect to the residual SDE. Intuitively, the non-identifiability breaks down when we start away from the two SDEs' shared stationary distribution, since the SDEs can then be identified by different rates of convergence to the stationary distribution, as shown in Figure 2.

Pair 2: Rotation around process mean

In this example, the residual SDE is given by

$$\frac{dX_t}{dt} = \begin{bmatrix} 0 & 1 \\ -1 & 0 \end{bmatrix} X_t \implies X_t = \begin{bmatrix} \cos(t) & \sin(t) \\ -\sin(t) & \cos(t) \end{bmatrix} X_0.$$

We can therefore validate non-identifiability if $X_0 \sim \mathcal{N}(0, Id)$, since $\begin{bmatrix} \cos(t) & \sin(t) \\ -\sin(t) & \cos(t) \end{bmatrix}$ corresponds to a counterclockwise rotation about the origin, and $\mathcal{N}(0, Id)$ is isotropic. Note that an initial distribution supported on just a single non-zero vector X_0 would suffice in identifying the rotation for this example since $\dim(\text{null}(A)) = 0$. This is shown in Figure 2 for $X_0 = (2, 0)$.

Pair 3: Degenerate Rank In this example, the residual SDE is given by

$$\frac{dX_t}{dt} = \begin{bmatrix} 2/3 & 2/3 \\ 1/3 & 1/3 \end{bmatrix} X_t.$$

If $X_0 = \begin{bmatrix} 1 \\ -1 \end{bmatrix}$ then X_0 is stationary with respect to the residual SDE since $dX_t = \begin{bmatrix} 2/3 & 2/3 \\ 1/3 & 1/3 \end{bmatrix} \begin{bmatrix} 1 \\ -1 \end{bmatrix} = 0$, as is the case for any X_0 in $\text{span}(\begin{bmatrix} 1 \\ -1 \end{bmatrix})$. However, if p_0 is supported on two linearly independent points, then it would be impossible to jointly achieve $dX_t = 0$ since $\dim(\text{null}(A)) = 1$. This is shown in Figure 2. Intuitively, this initialization resolves the non-identifiability by guaranteeing that both SDEs are observed on the entire space \mathbb{R}^d , whereas the previous initialization restricted observation to a linear subspace where the SDEs happened to behave equivalently.

Remark 8.16. We have seen that p_0 being stationary with respect to the residual SDE is a necessary condition for a pair of SDEs to be non-identifiable from p_0 . However, this condition is not sufficient. Two SDEs may be identifiable from p_0 despite p_0 being stationary with respect to the residual SDE. A simple example is given by a modification of the degenerate rank example.

$$dX_t = \begin{bmatrix} 1 & 2 \\ 1 & 0 \end{bmatrix} X_t dt + \begin{bmatrix} 1 & 0 \\ 0 & 1 \end{bmatrix} dW_t, X_0 = \begin{bmatrix} 1 \\ -1 \end{bmatrix} \quad (50)$$

$$dY_t = \begin{bmatrix} 1/3 & 4/3 \\ 2/3 & -1/3 \end{bmatrix} Y_t dt + \begin{bmatrix} 1 & 0 \\ 0 & 1 \end{bmatrix} dW_t, X_0 = \begin{bmatrix} 1 \\ -1 \end{bmatrix} \quad (51)$$

This pair of SDEs will have the same residual SDE as in the unidentifiable example, which is stationary with respect to $X_0 = \begin{bmatrix} 1 \\ -1 \end{bmatrix}$. However, by adjusting the diffusion to be full rank, this ensures that the processes will diffuse away from $\text{span}\left(\begin{bmatrix} 1 \\ -1 \end{bmatrix}\right)$, which would make the processes identifiable by their different behaviour away from this subspace.

8.5 Entropy-regularized Optimal Transport

The entropy-regularized optimal transport problem also admits a dual formulation, in terms of finding a pair of potentials (f, g) with respect to the Gaussian transition kernel $K(x, y) \propto e^{-\frac{c(x, y)}{\epsilon^2}} \propto e^{-\frac{\|y-x\|^2}{2\epsilon^2}}$ [Jan21, Nut21]:

$$\pi^*(x, y) = e^{f^*(x)+g^*(y)} K(x, y) d\mu(x) d\nu(y) \quad (52)$$

$$f^*, g^* = \sup_{f \in \mathcal{L}^1(\mu), g \in \mathcal{L}^1(\nu)} \mathbb{E}_\mu(f) + \mathbb{E}_\nu(g) - \left(\int_{\mathbb{R}^d \times \mathbb{R}^d} e^{f(x)+g(y)} K(x, y) d\mu(x) d\nu(y) - 1 \right). \quad (53)$$

In particular, given marginals μ, ν and the transition kernel K , Sinkhorn's algorithm uses the dual formulation (53) to find the ϵ -entropy regularized optimal transport solution π^* , by solving for f^*, g^* via iterative projections [PC⁺19].

Definition 8.17 (Markov concatenation of couplings). Given Polish spaces X_1, X_2, X_3 and couplings $\pi_{1,2} \in \mathcal{P}(X_1 \times X_2)$ and $\pi_{2,3} \in \mathcal{P}(X_2 \times X_3)$ with identical marginals μ_2 on X_2 , the Markov concatenation $\pi_{1,2} \circ \pi_{2,3}$ of $\pi_{1,2}$ and $\pi_{2,3}$ is a multi-coupling in $\mathcal{P}(X_1 \times X_2 \times X_3)$ given by

$$\pi_{1,2} \circ \pi_{2,3}(dx_1, dx_2, dx_3) = \pi_{1,2}(dx_1 | x_2) \mu_2(dx_2) \pi_{2,3}(dx_3 | x_2).$$

Here $\pi_{12}(dx_1 | x_2)$ is the disintegration of π_{12} with respect to μ_2 and $\pi_{2,3}(dx_3 | x_2)$ is the disintegration of $\pi_{2,3}$ with respect to μ_2 .

The interpretation of the Markov concatenation is as follows: a random ‘‘trajectory’’ according $\pi_{12} \circ \pi_{23}$ corresponds to taking the first two steps distributed according to π_{12} , then the third step distributed according to ‘‘ π_{23} conditional on the second marginal of π_{12} ’’. The existence of the Markov concatenation is guaranteed by the disintegration theorem, and Markov concatenations appear naturally in the time-discretized version of trajectory inference via Schrodinger bridges [LZKS21]. In particular, given Polish spaces X_1, \dots, X_4 and couplings $\pi_{12}, \pi_{23}, \pi_{34}$, it holds that Markov concatenation is associative, and so we can unambiguously define the iterated Markov concatenation $\pi_{12} \circ \pi_{23} \circ \pi_{34}$, see [BCDMN19] Section 3.2.

Proposition 8.18 (Optimality of anisotropic entropy-regularized optimal transport). Let the reference SDE be a linear additive noise SDE with drift A and diffusion H (2). Given a set of marginals p_0, \dots, p_{N-1} over times $\{t_i\}_{i=0}^{N-1}$ (not necessarily coming from the reference SDE) for which $D_{KL}(p_i | \text{Leb}) < \infty$ for all $1 \leq i \leq N-1$, and $D_{KL}(p_i | (p_{A,H})_i) < \infty$ for all $1 \leq i \leq N-2$, suppose there exists $\pi_{i,i+1}$, the anisotropic entropic OT solution (30) obtained by Sinkhorn's algorithm with marginals $\mu = p_i, \nu = p_{i+1}$ and transition kernel

$$K_{A,H}^i(x, y) \propto \exp\left(-\frac{1}{2}(y - e^{A(t_{i+1}-t_i)}x)^\top (\Sigma_i)^{-1} (y - e^{A(t_{i+1}-t_i)}x)\right) \quad (54)$$

where $\Sigma_i = \int_{t_i}^{t_{i+1}} e^{A(t_{i+1}-s)} H e^{A^\top(t_{i+1}-s)} ds$. Let π denote the joint distribution given by the Markov concatenation of couplings (see Definition 8.17):

$$\pi = \pi_{0,1} \circ \dots \circ \pi_{N-2,N-1},$$

Then, π minimizes relative entropy to the law of the reference SDE:

$$\pi = \arg \min_{\pi \in \Pi(p_0, \dots, p_{N-1})} D_{KL}(\pi \| p_{A,H}^N),$$

where $p_{A,H}^N$ is the law of the reference SDE, discretized over time points t_0, \dots, t_{N-1} .

Proof. For each $i = 0, \dots, N-1$, by (29), we have $\pi_i = \arg \min_{\pi \in \Pi(p_i, p_{i+1})} D_{KL}(\pi \| K_{A,H}^i)$. Since $K_{A,H}^i \sim \mathcal{N}(e^{A(t_{i+1}-t_i)} X_t, \Sigma_i)$ is the transition kernel of the SDE at time t_i [SS19][Sec 6.1], this implies that

$$\pi_i = \arg \min_{\pi \in \Pi(p_i, p_{i+1})} D_{KL}(\pi \| (p_{A,H})_{i,i+1}),$$

where $(p_{A,H})_{i,i+1}$ denotes the joint distribution of the marginals of $p_{A,H}$ at the two time points t_i, t_{i+1} . The details are as follows. Let $K_{i,i+1}(x, y)$ denote the transition kernel from time t_i to time t_{i+1} for the SDE $dX_t = AX_t + GdW_t$. In particular, if $(p_{A,H})_i$ is the marginal of this SDE at time t_i , then we have that $K_{i,i+1}(x, y)d(p_{A,H})_i(x)dy$ is equal to the joint distribution $(p_{A,H})_{i,i+1}$. Hence

$$D_{KL}(\pi | (p_{A,H})_{i,i+1}) = D_{KL}(\pi | K_{A,H}(x, y)d(p_{A,H})_i(x)dy).$$

We claim that for any $\pi \in \Pi(p_i, p_{i+1})$,

$$D_{KL}(\pi | K_{A,H}(x, y)d(p_{A,H})_i dy) = D_{KL}(\pi | K_{A,H}(x, y)dp_i(x)dp_{i+1}(y)) + D_{KL}(p_i | (p_{A,H})_i) + D_{KL}(p_{i+1} | \text{Leb}).$$

Indeed,

$$\begin{aligned} D_{KL}(\pi | K_{A,H}(x, y)d(p_{A,H})_i dy) &= \int \log \left(\frac{d\pi}{d(K \cdot (p_{A,H})_i \otimes \text{Leb})}(x, y) \right) d\pi \\ &= \int \log \left(\frac{d\pi}{d(K \cdot p_i \otimes dp_{i+1})}(x, y) \frac{d(K \cdot p_i \otimes dp_{i+1})}{d(K \cdot (p_{A,H})_i \otimes \text{Leb})}(x, y) \right) d\pi \\ &= \int \log \left(\frac{d\pi}{d(K \cdot p_i \otimes dp_{i+1})}(x, y) \frac{dp_i}{d(p_{A,H})_i}(x) \frac{dp_{i+1}}{d\text{Leb}}(y) \right) d\pi \\ &= D_{KL}(\pi | K_{A,H}(x, y)dp_i(x)dp_{i+1}(y)) + D_{KL}(p_i | (p_{A,H})_i) + D_{KL}(p_{i+1} | \text{Leb}). \end{aligned}$$

Note that $(p_{A,H})_0 = p_0$. Hence, under the assumption that for all $i = 1, \dots, N-1$, $D_{KL}(p_{i+1} | \text{Leb}) < \infty$, the minimizers for the following two minimization problems are identical:

$$\min_{\pi \in \Pi(p_i, p_{i+1})} D_{KL}(\pi | (p_{A,H})_{i,i+1}) \text{ and } \min_{\pi \in \Pi(p_i, p_{i+1})} D_{KL}(\pi | K_{A,H}(x, y)dp_i(x)dp_{i+1}(y)).$$

Since π is constructed as a Markov concatenation, the conclusion follows from Lemma 3.4 of [BCDMN19], which in this case tells us that: if $p_{A,H}^N$ is the projection of the law of the SDE onto the set of times $\{t_0, \dots, t_{N-1}\}$, then for any N -coupling π which is constructed as a Markovian concatenation $\pi_{0,1} \circ \dots \circ \pi_{N-2,N-1}$, and has i th marginal equal to p_i , we have

$$\text{KL}(\pi | p_{A,H}^N) = \sum_{i=0}^{N-2} \text{KL}(\pi_i | (p_{A,H})_{i,i+1}) - \sum_{i=1}^{N-2} \text{KL}(p_i | (p_{A,H})_i).$$

Hence minimizing over each $\text{KL}(\pi_{i,i+1} | (p_{A,H})_{i,i+1})$ (for $\pi \in \Pi(p_i, p_{i+1})$) is equivalent to minimizing over Markovian π 's with i th marginal p_i . □

8.6 Maximum Likelihood Estimation

Proof of Proposition (5.3). We follow the standard procedure [PMA03, Pav14] for deriving maximum likelihood estimators. Our likelihood function is given by

$$\mathcal{L} = \prod_{i=0}^{N-2} \left(\prod_{j=0}^{M-1} p(X_{i+1}^{(j)} | X_i^{(j)}) \right),$$

where we have denoted $X_i = X_{t_i}$ for shorthand. As in [Pav14], we consider the discretized law $X_{i+1}|X_i \sim \mathcal{N}(X_i + AX_i\Delta t, H\Delta t)$, which implies

$$p(X_{i+1}|X_i) = \frac{1}{(2\pi\Delta t)^d \det(H)^{1/2}} \exp\left(-\frac{1}{2}(\Delta X_i^{(j)} - AX_i^{(j)}\Delta t)^T (H\Delta t)^{-1} (\Delta X_i^{(j)} - AX_i^{(j)}\Delta t)\right),$$

where $\Delta X_i^{(j)} = X_{i+1}^{(j)} - X_i^{(j)}$. Plugging this back into the likelihood expression yields

$$\mathcal{L} = \frac{1}{(2\pi\Delta t)^{\frac{dM(N-1)}{2}} \det(H)^{\frac{M(N-1)}{2}}} \exp\left(-\sum_{i=0}^{N-2} \sum_{j=0}^{M-1} \frac{1}{2} (\Delta X_i^{(j)} - AX_i^{(j)}\Delta t)^T (H\Delta t)^{-1} (\Delta X_i^{(j)} - AX_i^{(j)}\Delta t)\right) \quad (55)$$

$$\log(\mathcal{L}) = -\frac{M(N-1)}{2} (d \log(2\pi\Delta t) + \log(\det(H))) - \frac{1}{2} \sum_{i=0}^{N-2} \sum_{j=0}^{M-1} \left(\Delta X_i^{(j)} - AX_i^{(j)}\Delta t \right)^T (H\Delta t)^{-1} \left(\Delta X_i^{(j)} - AX_i^{(j)}\Delta t \right) \quad (56)$$

We then derive the maximum likelihood estimators through matrix calculus [PP+08]:

$$\begin{aligned} \frac{d \log(\mathcal{L})}{dA} &= -\frac{1}{2} \sum_{i=0}^{N-2} \sum_{j=0}^{M-1} \frac{d}{dA} \left(\Delta X_i^{(j)} - AX_i^{(j)}\Delta t \right)^T (H\Delta t)^{-1} \left(\Delta X_i^{(j)} - AX_i^{(j)}\Delta t \right) \\ &= -\frac{1}{2} \sum_{i=0}^{N-2} \sum_{j=0}^{M-1} -2\Delta t \frac{d}{dA} \left((\Delta X_i^{(j)})^T (H\Delta t)^{-1} AX_i^{(j)} \right) + \Delta t^2 \frac{d}{dA} \left(X_i^{(j)T} A^T (H\Delta t)^{-1} AX_i^{(j)} \right) \\ &= -\frac{1}{2} \sum_{i=0}^{N-2} \sum_{j=0}^{M-1} -2\Delta t (H\Delta t)^{-1} (\Delta X_i^{(j)}) X_i^{(j)T} + 2\Delta t^2 (H\Delta t)^{-1} AX_i^{(j)} X_i^{(j)T} \\ &= \sum_{i=0}^{N-2} \sum_{j=0}^{M-1} (H)^{-1} (\Delta X_i^{(j)}) X_i^{(j)T} - \Delta t (H)^{-1} AX_i^{(j)} X_i^{(j)T} \end{aligned}$$

We can solve for the MLE linear drift A by setting $\frac{d \log(\mathcal{L})}{dA} = 0$:

$$\begin{aligned} \sum_{i=0}^{N-2} \sum_{j=0}^{M-1} \Delta t (H)^{-1} AX_i^{(j)} X_i^{(j)T} &= \sum_{i=0}^{N-2} \sum_{j=0}^{M-1} (H)^{-1} (\Delta X_i^{(j)}) X_i^{(j)T} \\ \Delta t (H)^{-1} A \sum_{i=0}^{N-2} \sum_{j=0}^{M-1} X_i^{(j)} X_i^{(j)T} &= (H)^{-1} \sum_{i=0}^{N-2} \sum_{j=0}^{M-1} \Delta X_i^{(j)} X_i^{(j)T} \\ A &= \frac{1}{\Delta t} \left(\sum_{i=0}^{N-2} \sum_{j=0}^{M-1} \Delta X_i^{(j)} X_i^{(j)T} \right) \left(\sum_{i=0}^{N-2} \sum_{j=0}^{M-1} X_i^{(j)} X_i^{(j)T} \right)^{-1} \end{aligned}$$

We now estimate the diffusion H . For simplicity, we work with $H^{-1} = (GG^T)^{-1}$

$$\begin{aligned} \frac{d \log(\mathcal{L})}{dH^{-1}} &= \frac{d}{dH^{-1}} \left(\frac{M(N-1)}{2} \log(\det(H^{-1})) - \frac{1}{2\Delta t} \sum_{i=0}^{N-2} \sum_{j=0}^{M-1} \left(\Delta X_i^{(j)} - AX_i^{(j)}\Delta t \right)^T H^{-1} \left(\Delta X_i^{(j)} - AX_i^{(j)}\Delta t \right) \right) \\ &= \frac{M(N-1)}{2} H - \frac{1}{2\Delta t} \sum_{i=0}^{N-2} \sum_{j=0}^{M-1} \left(\Delta X_i^{(j)} - AX_i^{(j)}\Delta t \right) \left(\Delta X_i^{(j)} - AX_i^{(j)}\Delta t \right)^T \end{aligned}$$

We can solve for the MLE additive noise H by setting $\frac{d \log(\mathcal{L})}{dH^{-1}} = 0$

$$\begin{aligned} H &= \frac{1}{M(N-1)\Delta t} \sum_{i=0}^{N-2} \sum_{j=0}^{M-1} \left(\Delta X_i^{(j)} - AX_i^{(j)}\Delta t \right) \left(\Delta X_i^{(j)} - AX_i^{(j)}\Delta t \right)^T \\ &= \frac{1}{MT} \sum_{i=0}^{N-2} \sum_{j=0}^{M-1} \left(\Delta X_i^{(j)} - AX_i^{(j)}\Delta t \right) \left(\Delta X_i^{(j)} - AX_i^{(j)}\Delta t \right)^T. \end{aligned}$$

□

Corollary 8.19. *Let X_t evolve according to a general additive noise SDE (1). Then the log-likelihood function is given by*

$$\mathcal{L} = \frac{1}{(2\pi\Delta t)^{\frac{dM(N-1)}{2}} \det(H)^{\frac{M(N-1)}{2}}} \exp \left(- \sum_{i=0}^{N-2} \sum_{j=0}^{M-1} \frac{1}{2} (\Delta X_i^{(j)} - b(X_i^{(j)})\Delta t)^T (H\Delta t)^{-1} (\Delta X_i^{(j)} - b(X_i^{(j)})\Delta t) \right)$$

$$\log(\mathcal{L}) = -\frac{M(N-1)}{2} (d \log(2\pi\Delta t) + \log(\det(H))) - \frac{1}{2} \sum_{i=0}^{N-2} \sum_{j=0}^{M-1} \left(\Delta X_i^{(j)} - b(X_i^{(j)})\Delta t \right)^T (H\Delta t)^{-1} (\Delta X_i^{(j)} - b(X_i^{(j)})\Delta t)$$

Hence, given that the drift function b is parameterized by values $\alpha_b^{(k)}$, the maximum likelihood solution for the drift function b obeys

$$0 = -\frac{1}{2} \sum_{i=0}^{N-2} \sum_{j=0}^{M-1} \frac{d}{d\alpha_b^{(k)}} \left(\Delta X_i^{(j)} - b(X_i^{(j)})\Delta t \right)^T (H\Delta t)^{-1} (\Delta X_i^{(j)} - b(X_i^{(j)})\Delta t)$$

The MLE for the diffusion H admits the closed solution

$$H = \frac{1}{MT} \sum_{i=0}^{N-1} \sum_{j=0}^{M-1} \left(\Delta X_i^{(j)} - b(X_i^{(j)})\Delta t \right) \left(\Delta X_i^{(j)} - b(X_i^{(j)})\Delta t \right)^T.$$

Proposition 8.20 (Exact MLE estimators for drift and diffusion of 1 dimensional SDE (2) from multiple trajectories). *Given M different trajectory time series over N different times: $\{X_{i+1}^{(j)} : i \in 0, \dots, N-1, j \in 0, \dots, M-1\}$ sampled from the linear additive noise SDE (2), the maximum likelihood solution for linear drift is approximated by*

$$\hat{A} = \frac{1}{\Delta t} \log \left(\frac{\sum_{i=0}^{N-2} \sum_{j=0}^{M-1} X_{i+1}^{(j)} X_i^{(j)}}{\sum_{i=0}^{N-2} \sum_{j=0}^{M-1} X_i^{(j)^2}} \right) \quad (57)$$

and the maximum likelihood solution for diffusion is approximated by

$$\hat{\sigma}^2 = \frac{1}{M(N-1)\Delta t} \sum_{i=0}^{N-2} \sum_{j=0}^{M-1} (X_{i+1}^{(j)} - e^{A\Delta t} X_i^{(j)})^2 \quad (58)$$

Proof. We proceed as in the proof of Proposition (5.3). The exact log-likelihood for the one dimensional case is

$$\log(\mathcal{L}) = -\frac{M(N-1)}{2} (\log(2\pi\Delta t) + \log(\sigma^2)) - \frac{1}{2\sigma^2\Delta t} \sum_{i=0}^{N-2} \sum_{j=0}^{M-1} (X_{i+1}^{(j)} - e^{A\Delta t} X_i^{(j)})^2$$

To solve for \hat{A} , we compute

$$0 = \frac{\partial \log(\mathcal{L})}{\partial A} \propto \sum_{i=0}^{N-2} \sum_{j=0}^{M-1} \frac{\partial}{\partial A} \left(-2X_{i+1}^{(j)} X_i^{(j)} e^{A\Delta t} + e^{2A\Delta t} X_i^{(j)^2} \right)$$

$$e^{2A\Delta t} \sum_{i=0}^{N-2} \sum_{j=0}^{M-1} X_i^{(j)^2} = e^{A\Delta t} \sum_{i=0}^{N-2} \sum_{j=0}^{M-1} X_{i+1}^{(j)} X_i^{(j)}$$

$$e^{A\Delta t} = \frac{\sum_{i=0}^{N-2} \sum_{j=0}^{M-1} X_{i+1}^{(j)} X_i^{(j)}}{\sum_{i=0}^{N-2} \sum_{j=0}^{M-1} X_i^{(j)^2}}$$

$$A = \frac{1}{\Delta t} \log \left(\frac{\sum_{i=0}^{N-2} \sum_{j=0}^{M-1} X_{i+1}^{(j)} X_i^{(j)}}{\sum_{i=0}^{N-2} \sum_{j=0}^{M-1} X_i^{(j)^2}} \right)$$

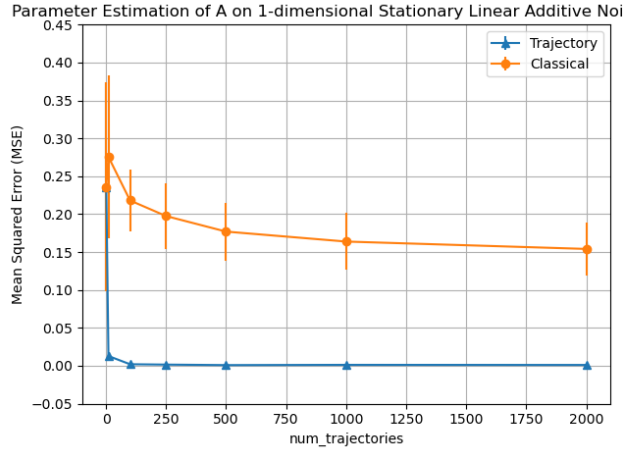


Figure 8: The expectation of the classical MLE drift estimator (Classical) converges at a slower rate compared to the MLE drift estimator (34) derived for multiple trajectories (Trajectory).

Similarly, to solve for $\hat{\sigma}^2$, we compute

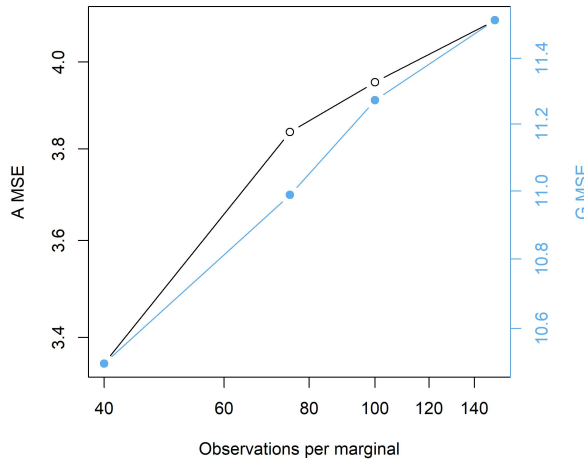
$$\begin{aligned}
0 &= \frac{\partial \log(\mathcal{L})}{\partial \sigma^2} \propto -\frac{M(N-1)}{2\sigma^2} + \frac{1}{2\Delta t} \frac{1}{(\sigma^2)^2} \sum_{i=0}^{N-2} \sum_{j=0}^{M-1} (X_{i+1}^{(j)} - e^{A\Delta t} X_i^{(j)})^2 \\
\frac{M(N-1)}{2} &= \frac{1}{2\Delta t \sigma^2} \sum_{i=0}^{N-2} \sum_{j=0}^{M-1} (X_{i+1}^{(j)} - e^{A\Delta t} X_i^{(j)})^2 \\
\sigma^2 &= \frac{1}{M(N-1)\Delta t} \sum_{i=0}^{N-2} \sum_{j=0}^{M-1} (X_{i+1}^{(j)} - e^{A\Delta t} X_i^{(j)})^2
\end{aligned}$$

□

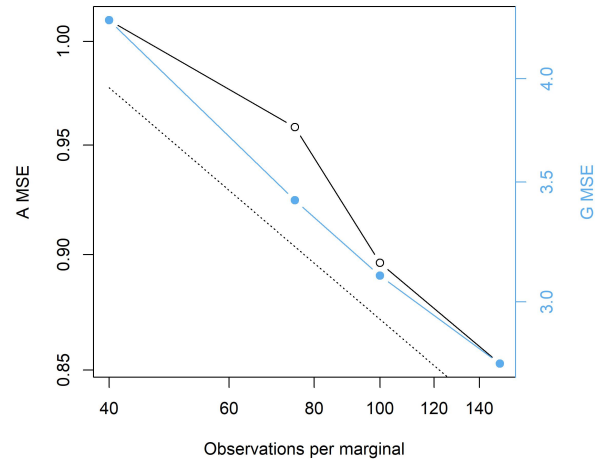
Remark 8.21. Previous works have predominately focused on the case of observing a single long trajectory rather than a collection of short trajectories. Suppose that one observes a set of N observed trajectories, then drift estimation may also be performed by averaging the classical MLE estimator for a single trajectory across observations: $\mathbb{E}_N[\hat{A}_T] = \frac{1}{N} \frac{\int_0^T X_t dX_t}{\int_0^T X_t^2 dt}$. Note that this is distinct from the MLE estimator that we derived for multiple trajectories in (34). Indeed, we observe that the latter estimator converges at a much faster rate than the averaged classical estimator.

9 Additional experiments

9.1 Consistency experiments

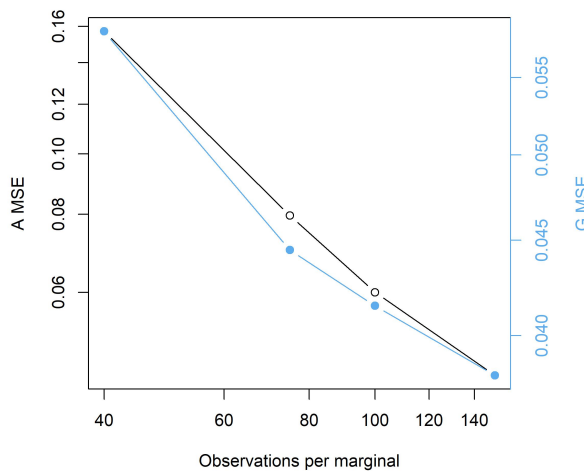


(a) WOT

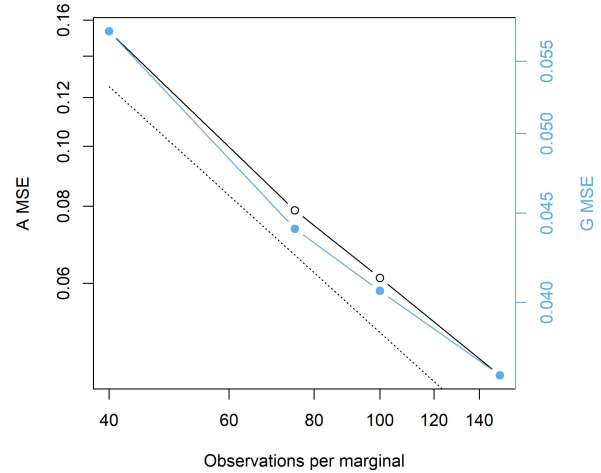


(b) GIMPI

Figure 9: Average mean squared error (MSE) of A and G as the number of observations per marginal increases across 50 random 2d systems. Note this is a log-log plot, and the dotted line in the GIMPI plot shows that the convergence follows a power law relationship with power -0.125 .



(a) WOT



(b) GIMPI

Figure 10: Average mean squared error (MSE) of A and G as the number of observations per marginal increases across 70 random 12d systems. Note this is a log-log plot, and the dotted line in the GIMPI plot shows that the convergence follows a power law relationship with power -1 .